Thermal anomaly in the Nacimiento Block, Monterey County, Central California: differential uplift or hydrothermal event?

by

Christine Marie Ward

B.S., Western State Colorado University, 2017

A THESIS

submitted in partial fulfillment of the requirements for the degree

MASTER OF SCIENCE

Department of Geology
College of Arts and Sciences

KANSAS STATE UNIVERSITY
Manhattan, Kansas

2020

Approved by:

Major Professor
Dr. Brice Lacroix

Copyright

Abstract

Within the Coastal Range of California one of the most significant stages in the geodynamics is the passage from subduction to transform motion between the Pacific and North American plates. The subduction of shallow asthenosphere is thought to trigger unusual heat flow, anomalous volcanism, and hydrothermal activities. Past post-subduction thermal overprints have been described in the Franciscan group from the Northern and Central California Coastal Ranges. To date, it is not clear whether the post-subduction thermal anomaly is a response to hydrothermal processes or to rapid vertical uplift by transpressive deformation. In this study we investigate the timing and kinematic processes controlling the thermal anomaly emplacement within the Nacimiento block between the San Gregorio Hozgri Fault (SGHF) and the Nacimiento fault in the Cape San Martin area. In order to address this question we applied (U-Th)/He thermochronological analysis on apatite and zircon grains from metasediments of the Nacimiento block to test whether the thermal anomaly observed resulted from a hydrothermal process or is a response to transpressive deformation. Coupled with Raman Spectroscopy on Carbonaceous Material (RSCM) thermometry on collected samples, we refined the peak temperature map proposed and performed a regional structural analysis to better understand how the thermochronological analysis results fit into the larger set of tectonic processes operating in the area. The results generated show that within the thermal anomaly the regional structures are oriented E-W, which significantly contrasts with the regional fabrics generally oriented N315°-N350°. This drastic orientation change suggests a counterclockwise rotation of about 50°- 75° compared to the regional fabrics. Our low-temperature (U-Th)/He thermochronological analyses show a distinct younging trend from the center of the thermal anomaly, from of 3.87 ± 0.28 Ma (apatite) and 11.77 ± 2.00 (zircon) Ma from the center of the thermal anomaly to 8.10 ± 1.60 (apatite) and 85.13 ± 13.09 Ma (zircon) at the outside edge of the thermal anomaly. Based on

these observations and inverse thermal modeling, we infer that the Nacimiento block has undergone subduction of a spreading center (triple junction). There is clear evidence within the Nacimiento block supporting the hypothesis of the subduction of a triple junction including: 1) plutons, 2) high-temperature, low-pressure metamorphic conditions, 3) dikes, and 4) quartz-calcite-sulfide mineralized veins located in the vicinity of the Los Burros Mining District (LBMD). Based on all of the above, we infer that the Nacimiento block is being affected by a combination of hydrothermal activities and transpressive deformation both as a result of subduction of a spreading center.

Table of Contents

List of Figures

List of Tables

Acknowledgements

First and foremost I would like to thank my advisor Dr. Brice Lacroix for pushing me every step of the way and always encouraging me to be the best that I can be. I greatly appreciate the many hours he has dedicated to helping me learn, grow, and understand my subject matter and myself as a researcher.

I would like to thank my committee members for all of their knowledge and help. A special thanks to Dr. Nathan Niemi and his lab manager Amanda Maslyn from University of Michigan for helping exponentially with my thermochronology sample preparation, analysis, and understanding of the subject matter. To Dr. Pamela Kempton for all of her support and feedback throughout this entire process and to Dr. Joel Spencer, for his humor and encouragement along the way.

I would like to thank the University of Michigan Thermochronology Lab for allowing me to utilize their lab to prepare and analyze my samples. I would also like to thank The Geological Society of America, the Nelson-Danheim Fellowship Fund, and Kansas State University for funding this project.

Dedication

This thesis is dedicated to my family for always encouraging me, listening to me, and providing endless advice throughout this entire journey. To my mom Terri for the countless phone calls, much needed advice, care packages, and visits. To my dad Fred for his matter of fact attitude and helpful home maintenance. To my grandma Pat for always sticking up for me and being my biggest supporter along the way. To my aunt Julie for understanding this entire process and always advising me to stick up for myself. To my uncle Steve for his humor and quick wit. I would also like to dedicate this to Brydie for continuously supporting me, encouraging me, and generally putting up with me through this entire experience. I could not have done this without every single one of you.

Chapter 1 - Introduction

One of the most significant stages in the geodynamics of the Coastal Range of California is the passage from subduction to transform motion between the Pacific and North American plates (Cole and Basu, 1995; Thorkelson, 1996; Underwood et al., 1999; Underwood and Laughland, 2001; Bradley et al., 2003; Lacroix et al., 2020). The subduction of shallow asthenosphere is thought to trigger unusual heat flow, anomalous volcanism, and hydrothermal activities (Dickinson and Snyder, 1979; Lachenbruch and Sass, 1980; Cole and Basu, 1995; Thorkelson 1996; Underwood et al., 1999; Underwood and Laughland, 2001; Haeussler et al., 2003; Bradley et al., 2003; Lacroix et al., 2020). Past post-subduction thermal overprints have been described in the Franciscan group from the Northern and Central California Coast Ranges (Underwood et al, 1995; Underwood and Laughland, 2001). A similar situation has been described in Southern Alaska, where a high-temperature metamorphism was superimposed on and took place after the regional subduction-related low-grade event (Dickinson and Snyder, 1979; Sisson et al. 1989; Bradley et al. 2003; Haeussler et al. 2003).

Using U-Pb detrital geochronology on detrital zircons, deposition within the Nacimiento block is estimated to have taken place 95 to 82 Ma (Lori, 2016; Chapman et al., 2016). HP-LT metamorphism is thought to have followed soon after, around 88 to 70 Ma, which was estimated using K-Ar radiometric ages on whole rock samples (Suppe and Armstrong, 1972; Ernst, 1980). In central California, Underwood et al. (1995) used vitrinite reflectance (R_o) (Figure 1.1) and illite crystallinity to propose that the Nacimiento block was affected by a post-metamorphic thermal anomaly (up to ~300°C). This later was confirmed by Lahfid et al. (2015) based on the Raman Spectroscopy of Carbonaceous Material (RSCM) geothermometer technique (Figure 1.1). Underwood and Laughland (2001) suggest that this post-subduction heating may be related to hydrothermal activity and ore deposition (e.g. the Los Burros Au-deposit) related to the

subduction of the Pacific plate under the North American plate. However, based on structural and fluid-inclusion analyses, Hughes (2018) demonstrates that the thermal anomaly and ore-deposition may not be linked. According to Hughes, (2018) the Los Burros Au-deposit formed at lower temperatures (>300 °C) than the peak temperature recorded by host sediments (>350 °C). In addition, Hughes (2018) suggests that the Los Burros deposit lies within a minor transpressive structure that extends from the adjacent San Gregorio Hozgri fault (SGHF) and Nacimiento fault. Although both the thermal anomaly and the Los Burros deposit seem spatially correlated, the regional peak temperature distribution is still poorly constrained. Most of the samples collected by Underwood et al. (1995) were collected along the coastline, leaving the thermal anomaly to be interpreted inland. Information on the ages of the thermal anomaly and ore deposit is required to understand the relationship between them.

Previous low-temperature thermochronological studies performed by Lori (2016) and Steely (2016) on samples from the Nacimiento block demonstrates that metasediments from the Franciscan group are suitable for thermochronological analysis of apatite and zircon grains. Unfortunately, sample locations included in these studies were designed to encompass regional scale tectonic processes and missed the thermal anomaly that is the focus of this study.

Interestingly, landslide mapping performed by the USGS demonstrates that the studied area is affected by higher landslide occurrences (Wills et al., 2003), including the Mud Creek Landslide on the Big Sur coast that occurred May 20, 2017 (Figure 1.2) (Gibbons et al., 2017). Two million cubic meters of rock and soil covered California State Highway 1 more than 65 feet deep and added about thirteen acres of land to the coast (Gibbons et al, 2017). Total cost to clear the highway was upwards of $40 million and took over a year to uncover. Due to the closure of HWY 1 for more than a year, this considerably impacted the local economy (Gibbons et al., 2017). Increased landslide activity could be occurring due to the hydrothermal activity or

differential uplift that could be affecting this area. Geomorphological studies would need to be done in order to link the landslides with our findings.

To date, it is not clear whether the post-subduction thermal anomaly is a response to hydrothermal processes or to rapid vertical uplift by transpressive deformation (as documented elsewhere in California) (Sorlien et al. 1999) between the SGHF and Nacimiento fault. In this study we investigate the timing and kinematic processes controlling the thermal anomaly emplacement within the Nacimiento block between SGHF and Nacimiento fault in the Cape San Martin area (Figure 1.3). In order to address this question we applied (U-Th)/He thermochronological analysis to apatite and zircon grains from sandstone metasediments of the Nacimiento block to test whether the thermal anomaly observed resulted from a hydrothermal process or is a response to transpressive deformation. We also applied Raman Spectroscopy on Carbonaceous Material (RSCM) thermometry (Lahfid et al., 2010) on collected samples to refine the peak temperature map proposed by Lahfid et el., (in prep.) and performed a regional structural analysis to better understand how the thermochronological analysis results fit into the larger set of tectonic processes operating in the area. The results generated by this project help us to understand the dynamics of transpressive deformation, which is assumed to affect the Nacimiento block and helped us to produce a detailed map of the post-subduction temperatures. They also helped generate a thermal history and uplift rate for the Nacimiento block as well as a structural map of the area.
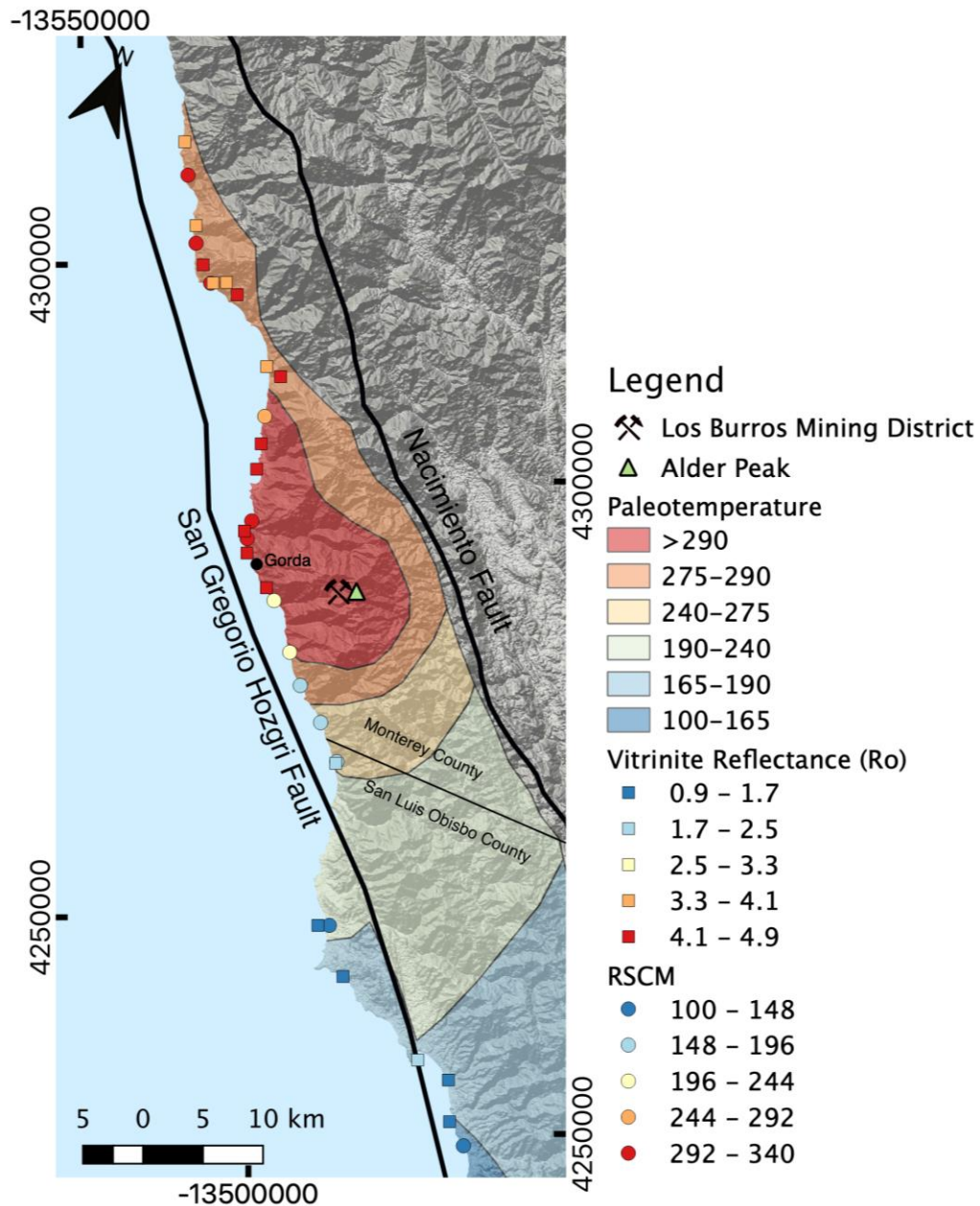
Figure 1.1 Map of Underwood et al. (1995) Ro data vs. Lahfid et al. (2015) RSCM data. Thermal maturity pattern for Franciscan rocks of the central California coast proposed by Underwood et al. (1995). *Figure modified from Underwood and Laughland (2001).*
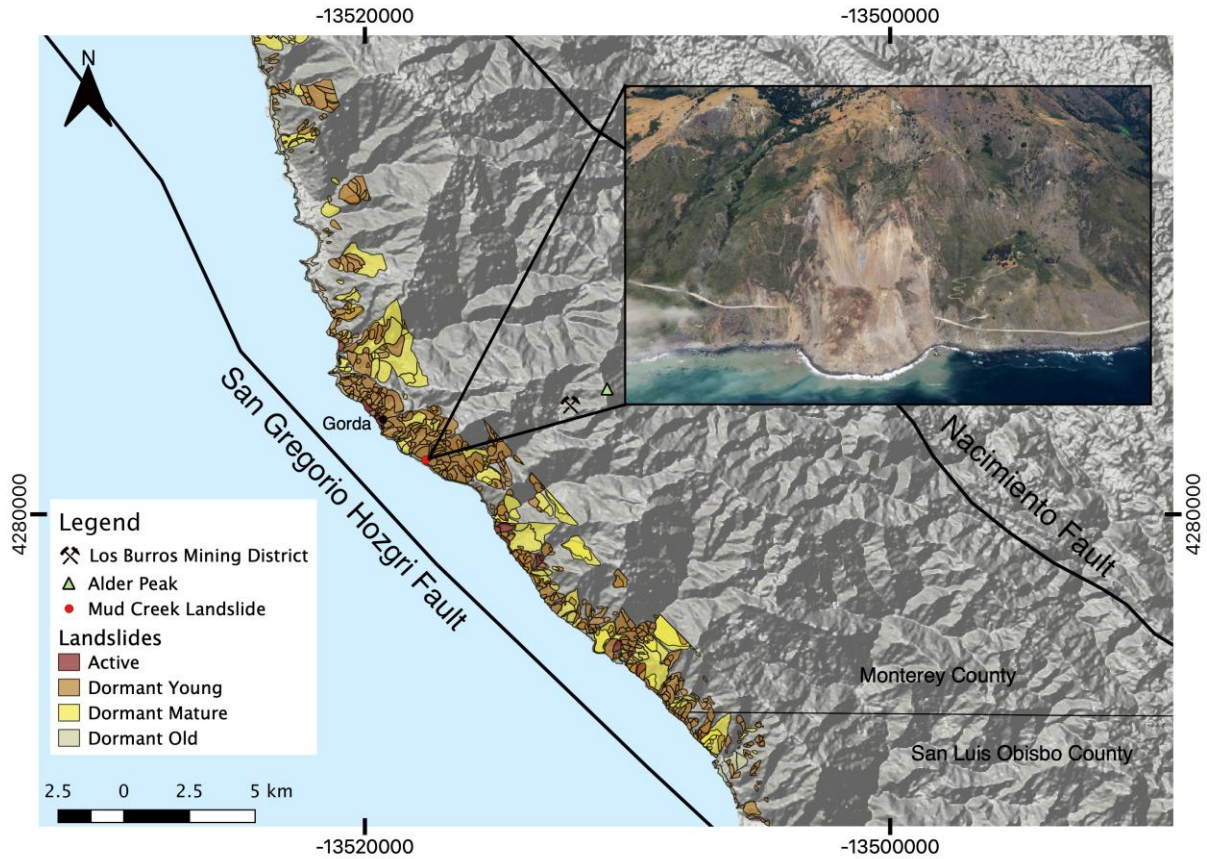
Figure 1.2 Landslide map of southern Monterey County, California, approximately 140 miles south of San Francisco. Study area is highly impacted by dormant young landslides. *Figure modified from Wills et al. (2003).*
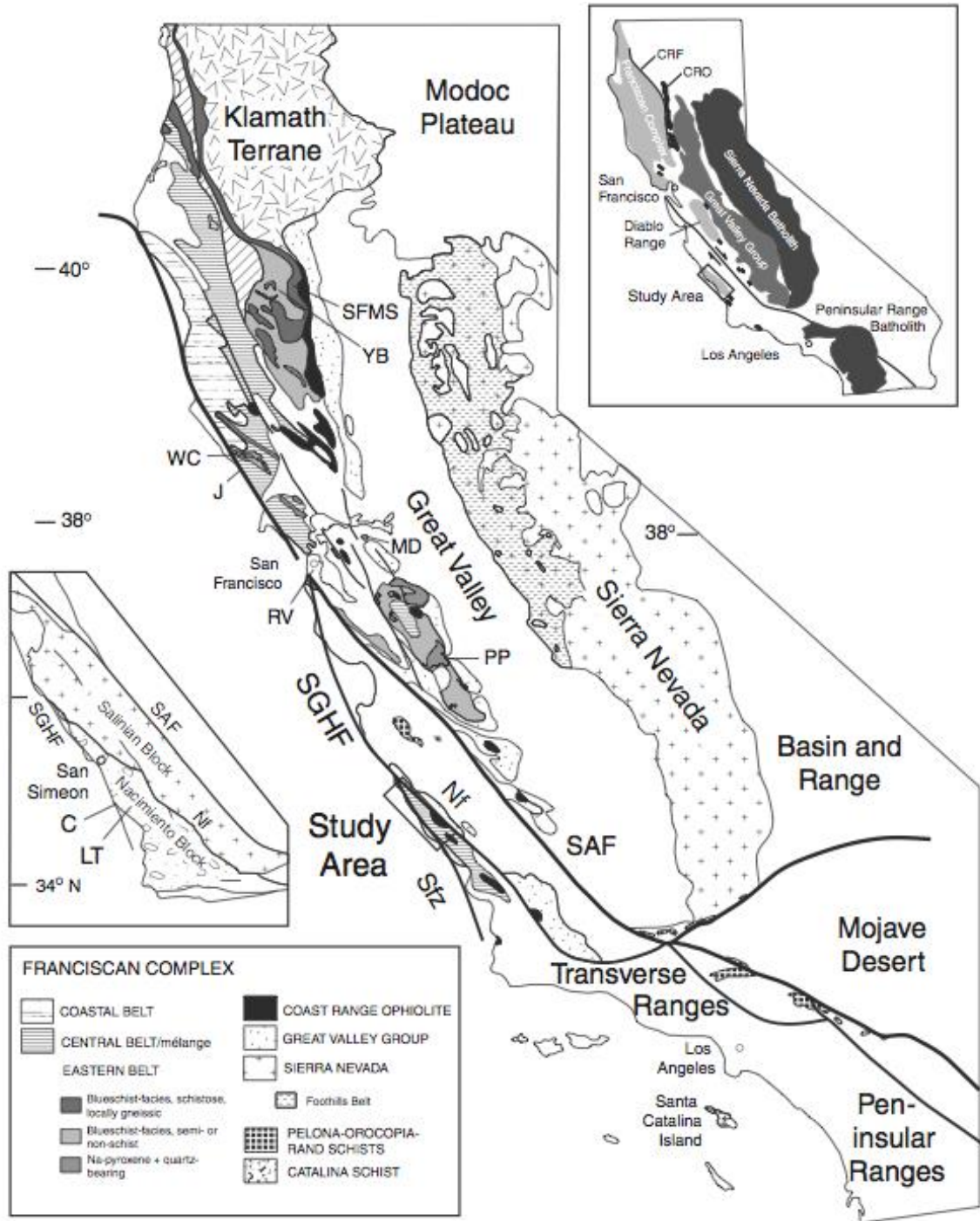
Figure 1.3 Schematic geologic map of California showing the three lithotectonic belts that make up most of the state: the Sierra Nevada and Peninsular Range batholiths, the Great Valley Group, and the Franciscan Complex, and the subdivisions of the different terranes. *Figure from Ukar (2012). C=Cambria; CRO=Coast Range Ophiolite; CRF = Coast Range Fault; J = Jenner; LT = Las Tablas; MD = Mount Diablo; Nf = Nacimiento Fault; PP = Pacheco Pas; RV = Rice Valley; SAF = San Andreas Fault; SGHF = San Gregorio Hosgri Fault; Sfz = Sur Fault Zone; SFMS = South Mountain Schist; YB = Yolla Bolly; WC = Ward Creek.*

6

Chapter 2 - Geologic and Tectonic Setting

2.1 - Tectonic setting

Our research area is located on the Nacimiento block near Cape San Martin, California, which is a component of the Franciscan subduction complex of the central California coast (Page, 1970; Underwood et al, 1995) (Figure 1.3). The Nacimiento block extends over a ~300 x 30 km area of the Coast Ranges and is bound to the south by the Santa Ynez fault and to the east by the Sur-Nacimiento fault (Page, 1970; Chapman et al., 2016). It is composed of late Jurassic to late Cretaceous Coastal Range ophiolitic accretionary wedge assemblages (Bailey et al., 1970; Jayko et al. 1987; Hall, 1991; Graymer et al., 2014; Chapman et al., 2016). The Nacimiento Franciscan Complex is a tectonic assemblage of sandstone, siltstone, shale, chert, conglomerate, serpentinite, and basaltic rocks, all of which are variably metamorphosed under high-pressure low-temperature conditions (Hsü, 1969; Gilbert, 1973; Cowan and Page, 1975; Ernst, 1980; Underwood et al., 1995; Underwood and Laughland, 2001; Graymer et al., 2014; Chapman et al., 2016). Based on mineralogy and bulk rock compositions, Ernst (1980) classified the Nacimiento block into three metamorphic zones and determined that there was an increase in temperature and degree of metamorphism to the northeast (Figure 2.1) (Ernst, 1980; Chapman et al., 2016). Zones from west to east: zone I – characterized by calcite with no new Ca-Al hydrous silicates; zone 2 – pumpellyite bearing; and zone III – lawsonite ± aragonite ± jadeitic pyroxene-bearing (Figure 2.1) (Ernst, 1980; Chapman et al., 2016). The Nacimiento block is hypothesized to have undergone a recrystallization event during subduction under temperatures of ~150-300 °C at lithostatic pressures ranging from 2 to 3 kbar in the west to 5 to 8 kbar in the east (Ernst, 1980; Chapman et al., 2016). The Nacimiento Franciscan can be divided into three distinct units: "(1) broken formation consisting of internally sheared yet coherent well-bedded sandstone and turbidite sequences that lack exotic blocks; (2) a chaotically sheared (mélange) unit mainly

consisting of clastic and greenstone blocks within a foliated siliciclastic matrix and containing <1% exotic blocks of chert, blueschist, and serpentinite; and (3) coherent unmetamorphosed submarine fan systems interpreted as trench-slope basin assemblages (slabs) lying in depositional contact above, and containing detritus from, the subduction complex." (Chapman et al., 2016).

K-Ar radiometric ages on three whole rock samples of Lucia area metagraywackes yield ages of 70, 74, and 88 Ma, supporting the hypothesis of a Late Cretaceous metamorphic recrystallization event (Suppe and Armstrong, 1972; Ernst, 1980). Deposition ages of the Franciscan rocks from the Nacimiento block, which range from 95 to 82 Ma, were estimated using U-Pb geochronology on detrital zircons (Lori, 2016; Chapman et al., 2016). The onset of subduction in the Nacimiento block is thought to be constrained by the 120-100 Ma metamorphosed blueschist blocks in mélange near San Simeon (Chapman, 2016). The small time lapse between these radiometric ages suggests that regional subduction-related metamorphism occurred shortly after deposition/sedimentation of sediments for the Nacimiento block (Suppe and Armstrong, 1972; Ernst, 1980; Chapman et al., 2016).

The origin of the Nacimiento block is still highly debated. Chapman et al. (2016) found that there were abundant of Late Cretaceous detrital zircon grains in the Nacimiento block. This suggests that the Sierra Nevada-Peninsular Ranges originated to the south, indicating a total offset of ~150 – 160 km (Figure 1.3) (Clark, 1998; Chapman et al., 2016). This follows the idea that there is a relative younging trend (Early Cretaceous to middle Miocene) to the south and west of the northern Coast Ranges and San Francisco Bay Area (Ernst, 2015; Chapman et al., 2016). In contrast, based on temperature isograd correlation, Underwood et al. (1995) suggests that there was no more than 5-10 km of Neogene and Quaternary dextral offset between the Big Sur and Nacimiento blocks along the SGHF zone (Figure 1.1) (Underwood et al., 1995). These authors argued that the dextral offset could either be accommodated via a single fault system or a

series of fault segments, but because they could not trace the faults offshore they could not determine which fault system they were observing.
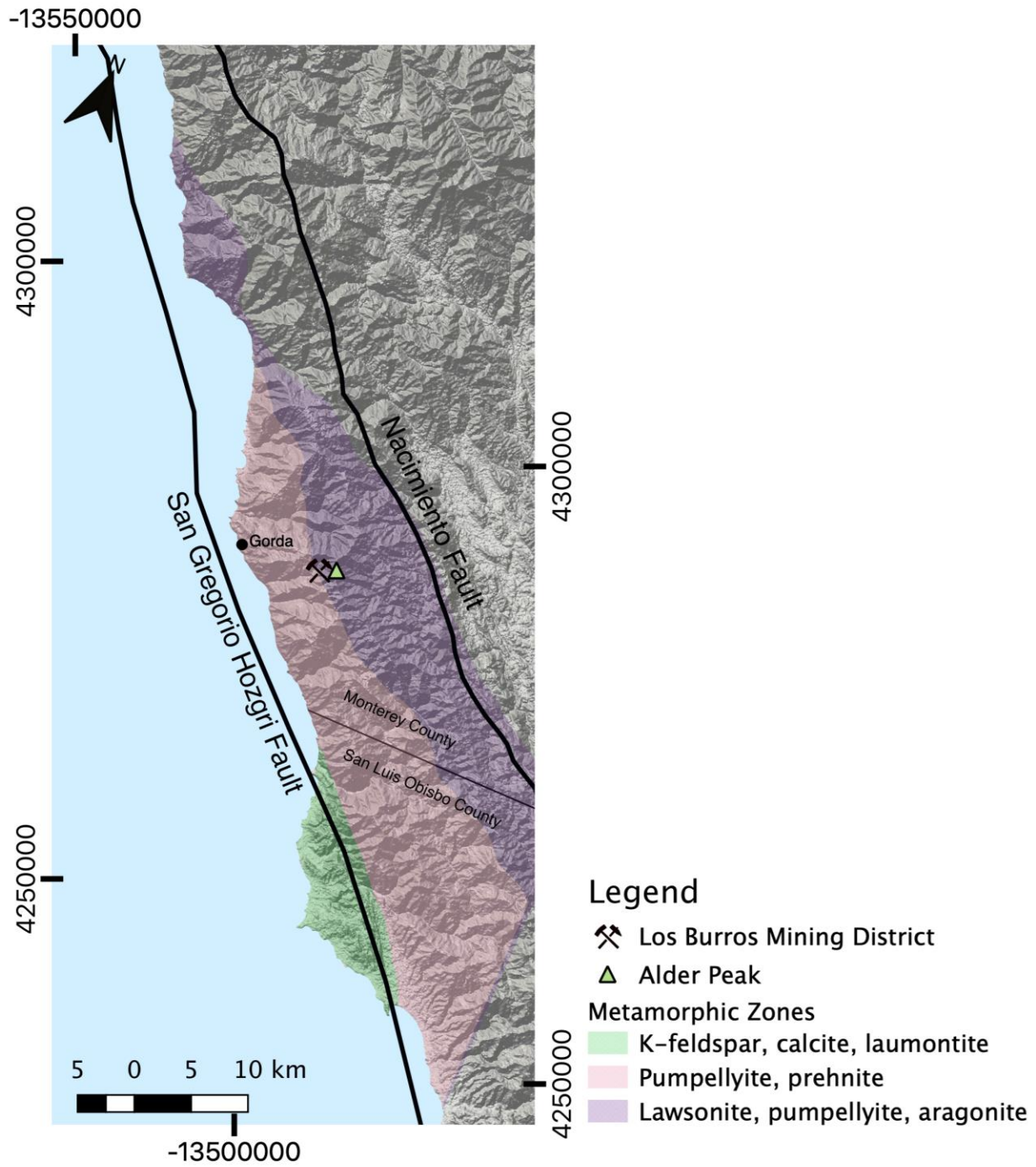
Figure 2.1 Franciscan metamorphic zones from Ernst (1980). *Figure modified from Underwood et al. (1995).*

2.2 - Thermal anomaly

Underwood et al. (1995) used vitrinite reflectance (R_o) and illite crystallinity methods on metasediments from the Franciscan complex to propose that the Nacimiento block is affected by a local thermal anomaly (up to ~300°C) (Figure 1.1). More recently, Lahfid et al. (2015) expanded on this idea of a thermal anomaly by use of the RSCM geothermometer to confirm the presence of a thermal anomaly in this area (Figure 1.1), demonstrating that this technique is suitable in the context of HP metamorphism. Underwood and Laughland (2001) link this anomaly to post subduction heating, possibly related to hydrothermal activity and ore deposition (Los Burros Mining District). Post subduction heating is likely due to triple junction subduction that is thought to have caused the evolution of the San Andreas Fault along the California coastline and cause a slab-free region beneath the continent adjacent to the transform fault (Dickinson and Snyder, 1979). More recently, Hughes (2018) proposed that the Los Burros gold deposit, located within the study area and within the proposed thermal anomaly, lies within a minor, transpressive ridge structure due to the successive compressional and translational stresses applied in the region (Figure 2.2). Structural reorientation has been observed within the Nacimiento block by Lacroix et al. (2020); however, it was locally within the Los Burros mining district (Figure 2.3), so more data need to be collected to complete a regional structural analysis on the Nacimiento block.

In this study we apply thermochronology to sandstone metasediments of the Nacimiento block to test whether the thermal anomaly observed by Underwood et al. (1995) and Lahfid et al. (2015) resulted from a hydrothermal process or is a response to transpressive deformation as hypothesized by Hughes (2018). RSCM was performed on shale collected close to the thermochronology samples to allow for a temperature constraint on the samples.
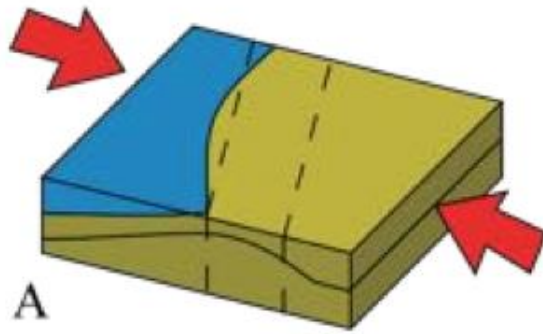
Visualization of compressional forces due to subduction. Deformation and faulting associated with event 1. Uplift begins.
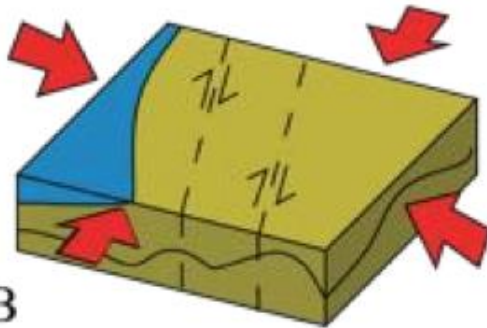
Compressional and translational forces related to event 1 and event 2, respectively. Reactivation of faults with dextral motion.
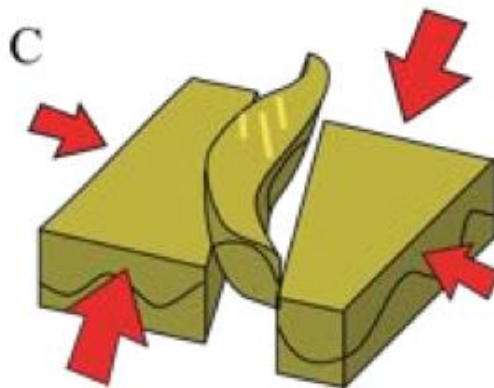
Compressional forces become less significant relative to translational forces. Combination of event 1 and event 2 deformation leads to uplift and rotation of transpressional "pop-up". Gold emplacement occurs.

Figure 2.2 Block diagram representing structural controls on the northern Nacimiento block near the Los Burros Mining District, including gold deposition. *Figure modified from Hughes (2018).*
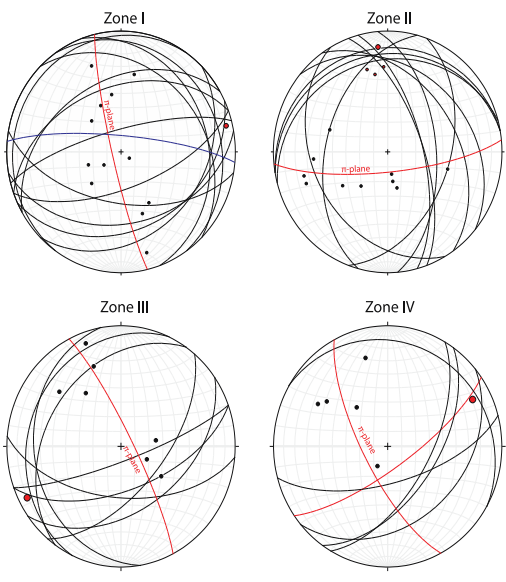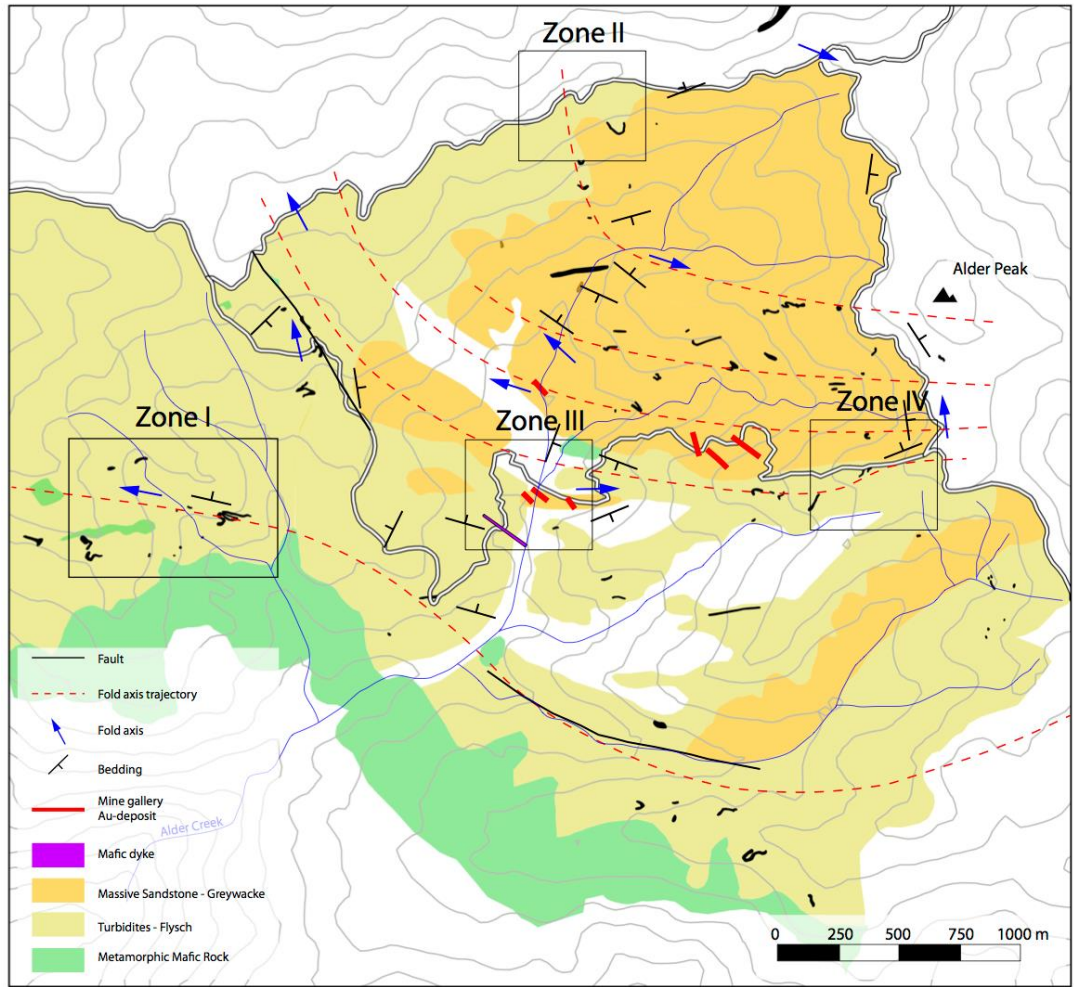
Figure 2.3 Map of Lacroix et al. (2020) structural data showing structural reorientation in the Los Burros mining district. Counterclockwise rotation of about 50°- 75° was observed from the regional trend of N315°-N350°. *Figure from Lacroix et al. (2020).*

Chapter 3 - Methodology

3.1 - Fieldwork

In this project, we adopt a multi-disciplinary approach including fieldwork, sample collection, and a detailed (U-Th)/He thermochronological analysis on apatite and zircon grains to understand the tectonic processes responsible for the thermal anomaly and the observed structural re-orientation. Fieldwork included structural analysis and sampling of rock belonging to the Franciscan group, a series of carbonaceous-rich sediments metamorphosed within the three metamorphic facies described in Ernst (1980). These rocks include detrital and metamorphic K-feldspars and zircons having Cretaceous (90-70 Ma) peak metamorphic ages (Suppe and Armstrong, 1972). Preliminary analysis on samples from the Nacimiento block demonstrates that metasediments from the Franciscan group are suitable for thermochronological analysis of zircons (Lori, 2016). Greywacke or sandstone samples were collected along a cross-section across the thermal anomaly identified by Underwood and Laughland (2001) and Lahfid et al. (in prep.) using dirt roads and hiking trails (Figure 3.1). One sample was also collected far from the thermal anomaly and hypothesized transpressive deformation in order to obtain an age background for the Franciscan group prior to the thermal anomaly emplacement (Figure 3.1). All samples were collected near locations that had previously been analyzed by the RSCM method by Lahfid et al. (in prep) or where RSCM samples could be collected nearby to help constrain the temperature of the thermochronology samples. A summary of the samples collected can be found in Table 3.1. About 1 kg of rock was collected and GPS coordinates and elevations recorded by a field tablet from the department of Geology (accuracy <2 meters). Samples were carefully inspected in the field to ensure limited impacts from alteration, particularly weathering that might have affected the apatite and zircon grains. Samples were labeled and carefully packed and shipped to the University of Michigan for further preparation. Fieldwork was also dedicated to

structural analysis and mapping to document the orientation of the principal fabric (folds, schistosity, faults, etc.) and to document structure rotation as described by Storti et al. (2003). Regional structural analysis of the Nacimiento block was performed integrating structural data collected in the field, published structural data (eg. Graymer et al., 2014), and by completing a structural interpretation of tectonic features (bedding, fault, fold) from a satellite Google image.
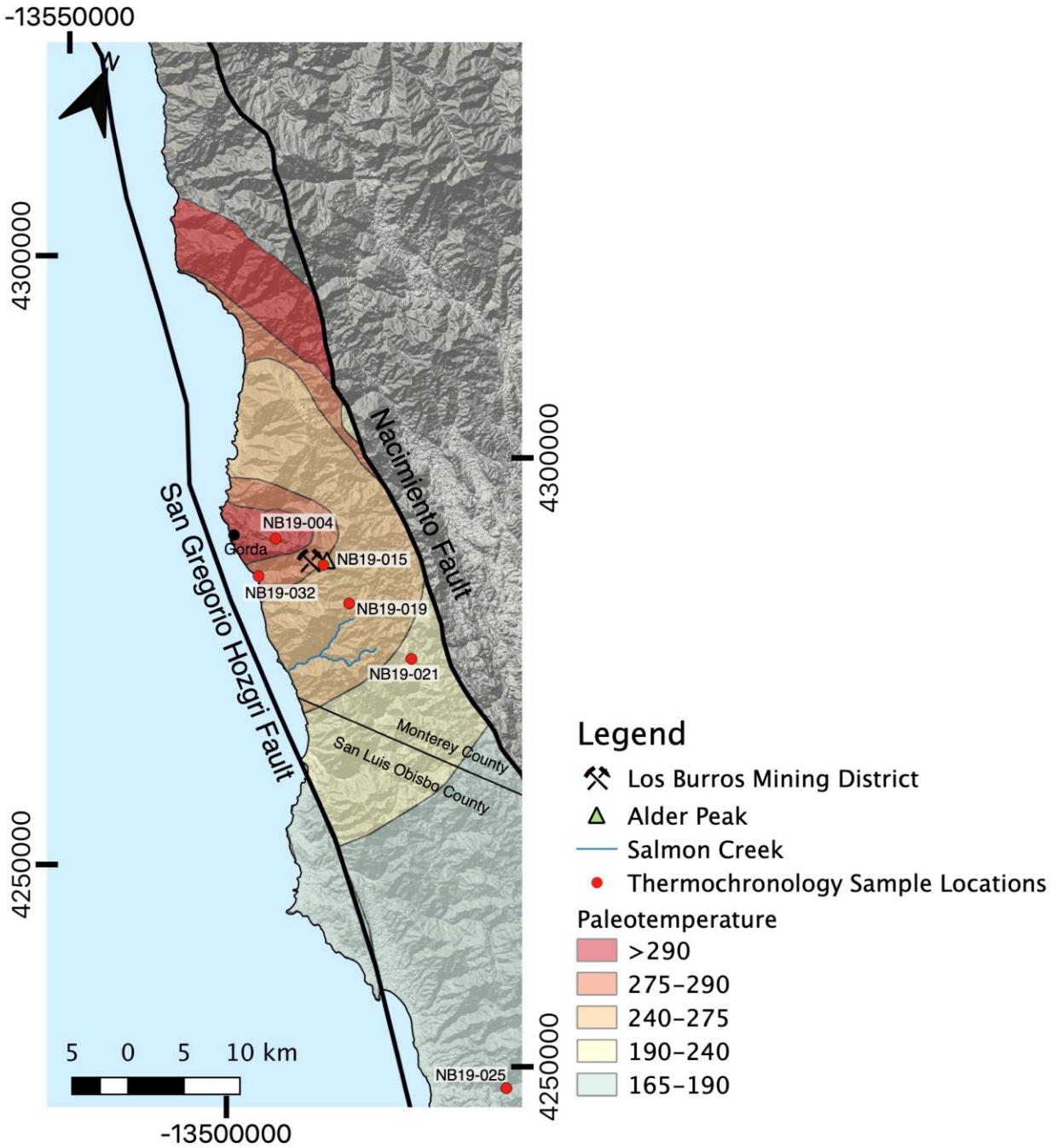
Figure 3.1 Map showing locations of samples collected for thermochronological analysis. Paleotemperature contours interpreted from RSCM data from Lahfid. Sample names indicated next to each sample location.

Table 3.1 Summary of samples collected during fieldwork.

Map ID/ Sample #	Latitude/Longitude	Elevation (m)	Sample Type	Sample Analysis
NB19-004	35.8847, -121.414	810	Greywacke and Carbonaceous-rich metasediment	(U-Th)/He Thermochronology and RSCM
NB19-015	35.8811, -121.371	1057	Sandstone and Carbonaceous-rich metasediment	(U-Th)/He Thermochronology and RSCM
NB19-019	35.8646, -121.339	935	Sandstone and Carbonaceous-rich metasediment	(U-Th)/He Thermochronology and RSCM
NB19-021	35.8472, -121.276	781	Sandstone and Carbonaceous-rich metasediment	(U-Th)/He Thermochronology and RSCM
NB19-025	35.6142, -121.071	59	Sandstone and Carbonaceous-rich metasediment	(U-Th)/He Thermochronology and RSCM
NB19-031	35.8546, -121.411	51	Carbonaceous-rich metasediment	RSCM
NB19-032	35.8579, -121.415	30	Sandstone and Carbonaceous-rich metasediment	(U-Th)/He Thermochronology and RSCM

3.2 - Raman Spectroscopy on Carbonaceous Material (RSCM)

RSCM analysis was done on four carbonaceous-rich metasediment samples (NB19-031 A-D) located near an intrusion near the center of the thermal anomaly. The stable form of elemental carbon at the Earth's surface and in the crust is graphite but well-crystallized graphite is relatively rare (Buseck and Beyssac, 2014). More commonly we observe a poorly crystallized, disordered material commonly called "carbonaceous material" (Beyssac et al. 2002; Lahfid et al., 2010; Buseck and Beyssac, 2014). Graphitization and carbonization are the names given to the progressive, irreversible transformation of disordered or partly ordered, noncrystalline carbon-bearing material into pure carbon, with the end member being crystalline graphite (Buseck and Beyssac, 2014). Incomplete graphitization, which is common, results in carbonaceous materials having different degrees of crystallographic order, which arise from various combinations of temperature, pressure, kinetics, and, in some cases, fluid activity (Buseck and Beyssac, 2014). Based on the Raman approach, Beyssac et al. (2002) quantified the graphitization and carbonization processes of carbonaceous material and calibrated the Raman Spectroscopy of Carbonaceous Material (RSCM) geothermometer (Beyssac et al. 2002; Lahfid et al., 2010). RSCM measures the structural evolution of the carbonaceous material that is present in rocks (Beyssac et al. 2002; Lahfid et al., 2010). The version of the RSCM technique used in this study was developed by Lahfid et al. (2010) on carbonaceous material that experienced low temperatures ranging from 200 to 350°C.

Whole rock samples were cut ~0.5 inch thick to expose a fresh unaltered surface for RSCM analysis. RSCM was performed at the Department of Geology (KSU) on cut whole rock samples using a Renishaw in Via Reflex microspectrometer system equipped with a 514 nm Spectra Physics (20mW) argon laser. The Raman spectrometer was operated using a continuous scanning mode with large spectral windows from 700 to 2000 cm^{-1}. This spectral range is the

minimum required to image the whole background signal clearly and define the baseline properly (Lahfid et al., 2010). Instrument control and Raman measurements were performed with the software packages Renishaw Wire. The acquisition times while using this software is generally over 10 seconds (Lahfid et al., 2010). In this study each cut whole rock sample was exposed to a laser beam with power of around 0.5 mW at the sample surface. To check the structural heterogeneity within each sample, at least 15-20 spectra were recorded per sample. During peak fitting of carbonaceous material spectra, we followed Lahfid et al. (2010) which utilizes the Lorentzian profiles (Bonal et al., 2006) and the five-band combination of Lorentzian/Gaussian profiles (Sadezky et al., 2005) for the peak fitting procedure because they reduce the degree of freedom of the system and because all of the bands systematically converge rapidly towards a unique solution. This fitting procedure is represented in Figure 3.2. Based on this peak fitting procedure Lahfid et al. (2010) found that two area ratios best described the evolution of the Raman spectrum with increasing metamorphic grade. The two equations RA1 = (D1 + D4)/(D1 + D2 + D3 + D4 + G) and RA2 = (D1 + D4)/(D2 + D3 + G) were selected as they exhibit the most significant evolution with acceptable errors, which are equal to the standard deviation for *n* spectra (Lahfid et al., 2010). These two ratios may be used as the quantitative representations for the degree of carbonaceous material organization in low-grade metamorphism because they progressively increase with increasing metamorphic grade (Lahfid et al., 2010). In this study we only utilized the first of the two equations RA1 = (D1 + D4)/(D1 + D2 + D3 + D4 + G) because we followed the same procedure utilized in Lahfid et al. (2015) on samples from the Nacimiento block, where he only focused on the RA1 value. There is a direct relationship between the RA1 ratio and temperature; this can be seen in Figure 3.3 (Lahfid, 2010).

There are some issues with this technique that may control the evolution of Raman spectra of carbonaceous material in low-grade metamorphism (Lahfid et al., 2010). At higher

metamorphic grade (T > 350 °C), temperature has been shown to be the only parameter
controlling graphitization during metamorphism (Beyssac et al., 2002; Lahfid et al., 2010).
Whereas at low temperature metamorphism, temperature, pressure, time, the nature of the
precursor material and even deformation may affect the structure of the carbonaceous material
(Lahfid et al., 2010). However, this technique has already been applied on metasediments from
the Nacimiento block (Figure 3.4) (Lahfid et al., 2015). Lahfid et al. (2015) tested his low-
temperature RSCM technique where Underwood et al. (1995) had already done vitrinite
reflectance in the area, and confirmed the increase in metamorphic grade towards the north.
Based on the results of this study Lahfid et al. (2015) suggests that RSCM could be used as a
reliable tool to explain thermal anomalies induced by hot fluid-flow. RSCM data are useful with
regards to thermochronology, because they constrain the maximum peak temperature reached by
the rock and, thus, refine the temperature vs. time models.
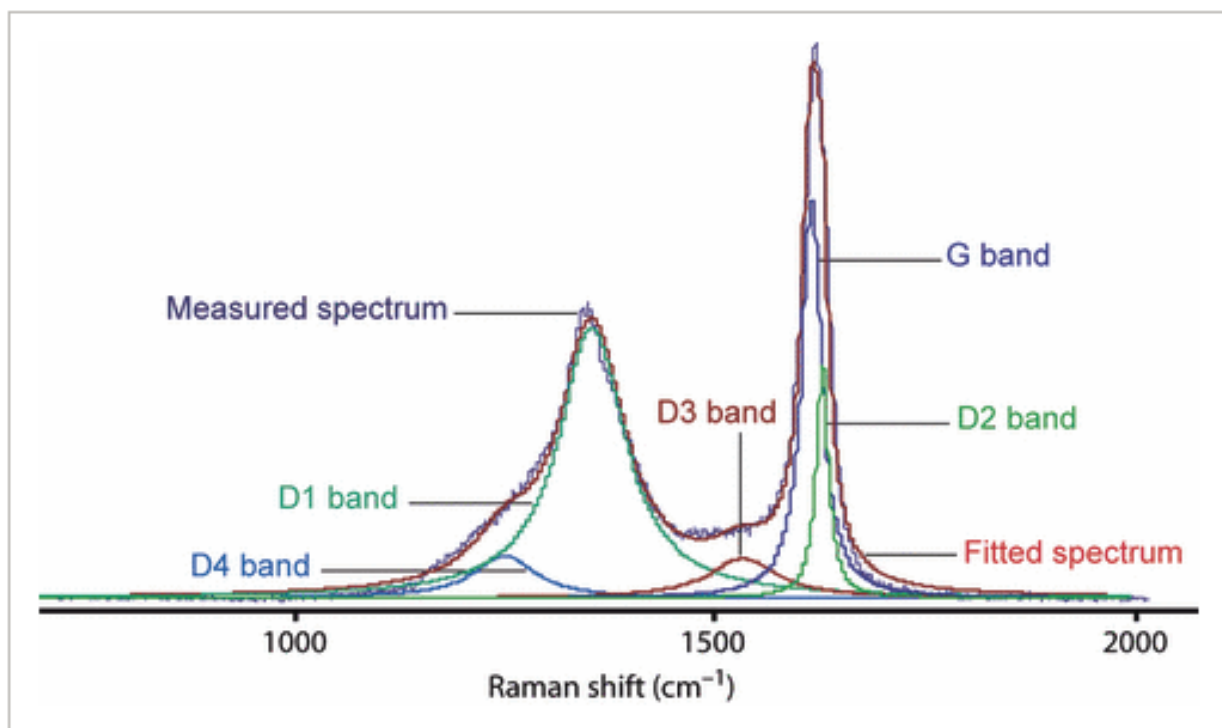
Figure 3.2 Peak-fitting of the Raman spectrum of disordered carbonaceous material from low-grade metamorphic rocks. This spectrum is composed of a G band (graphite band) and the various D bands. For peak-fitting, each of the five bands have a pure Lorentzian shape and no *a priori* restriction is imposed on the band position. *Figure from Lahfid et al. (2010).*
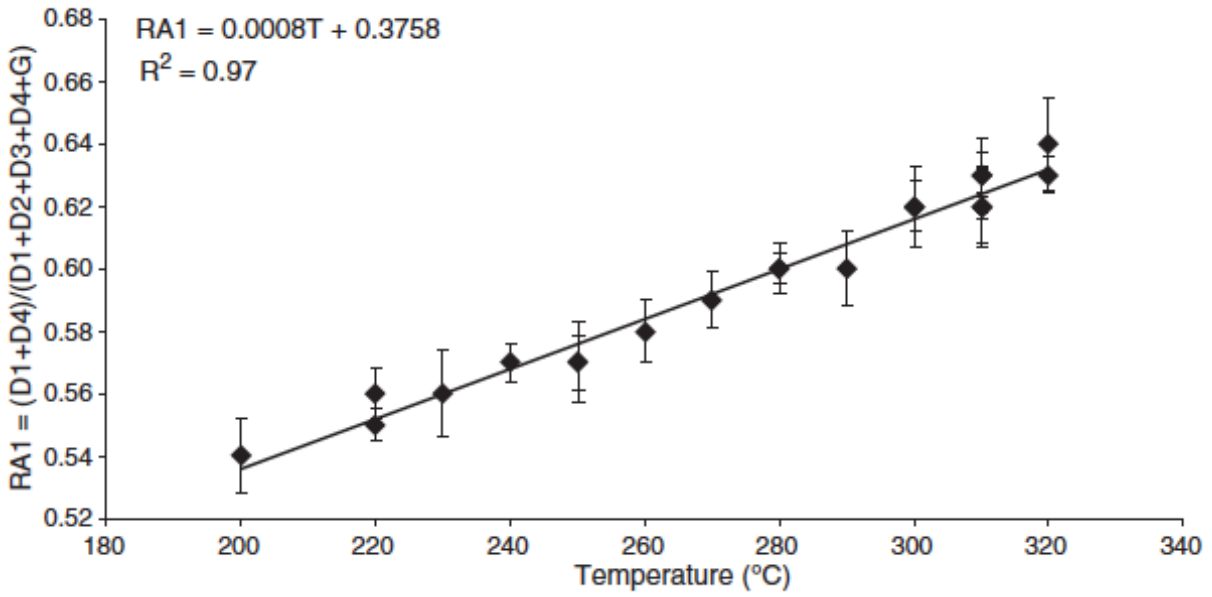
Figure 3.3 Evolution of the RA1 ratio with temperature in the Glarus Alps. RA1 = (D1 + D4)/(D1 + D2 + D3 + D4 + G) area ratio. *Figure from Lahfid et al. (2010).*
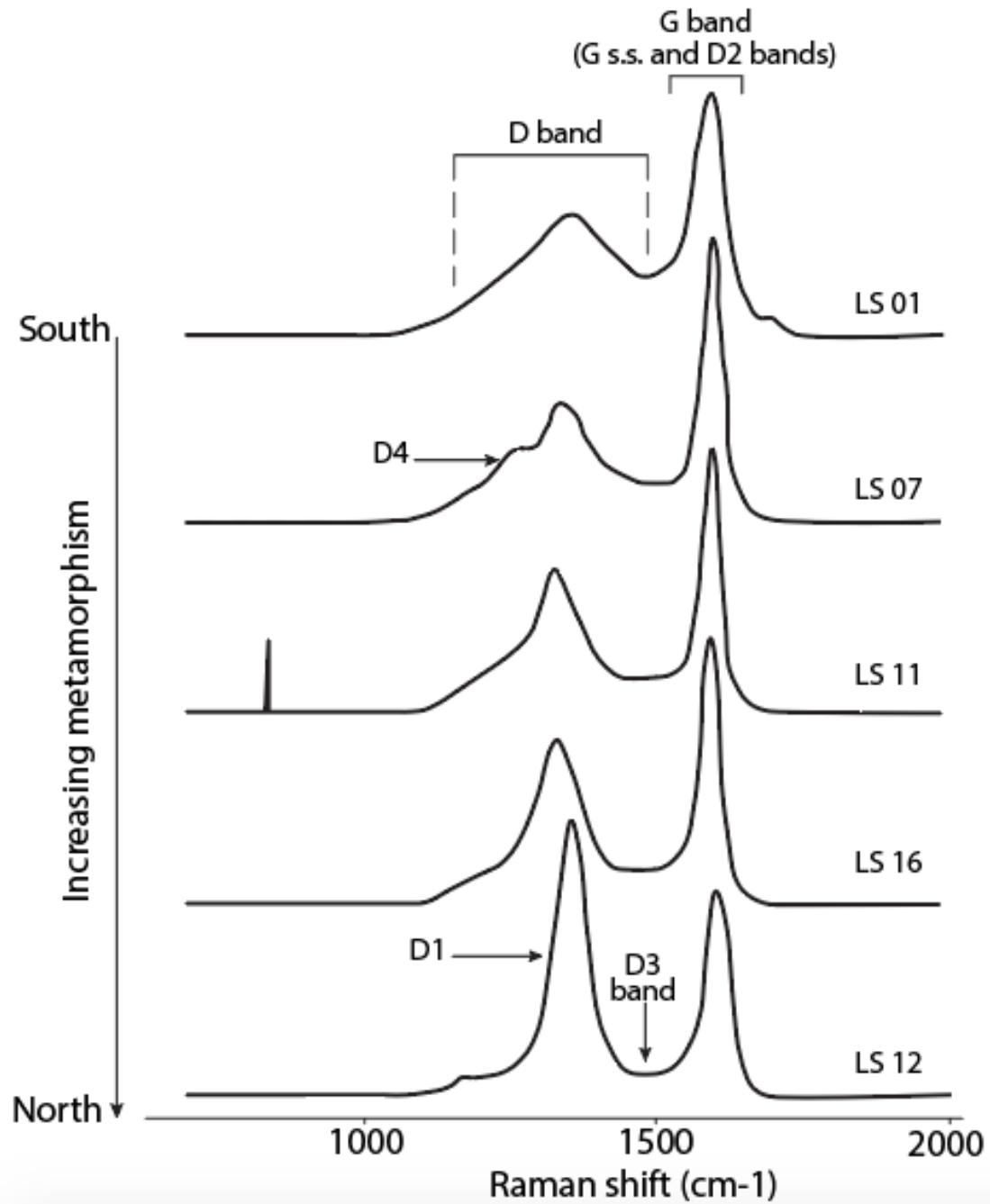
Figure 3.4 Representative Raman spectra of carbonaceous material of samples collected from the Nacimiento block Lucia subterrane. *Figure modified from Lahfid et al. (2015).*

3.3 - Thermochronological Analysis

Thermochronological analysis was done on greywacke and sandstone metasediment rock samples (NB19-004, NB19-015, NB19-019, NB19-021, NB19-025, NB19-032). Using a standard mineral separation technique described in Chapman et al. (2016), the greywacke and sandstone metasediment rock samples were crushed, sieved, processed with a magnetic separator and through heavy liquids, and finally handpicked using a binocular microscope. Zircon and apatite grains were selected to undergo thermochronological analysis at the University of Michigan's Thermochronology Lab.

To date the zircon and apatite grains, approximately 3-4 apatite grains and 3 zircon grains were selected per sample. Zircon and apatite grains were selected for (U-Th)/He dating based on shape and size, following the criteria of Reiners (2005) and Lori (2016), i.e. grains must be euhedral-subhedral, and grains must be representative of the average size of mineral from that particular sample with the length of grain axes no smaller than 60 microns. After handpicking, the length of each grain was measured along all three axes and packed into a Nb capsule where it was processed for He extraction in an Alphachron Helium Instrument. Then, mineral grains were sent to University of Arizona where they were dissolved in Teflon ^{TM} bombs for parent isotope (U and Th) analysis in a ThermoFinnigan Element 2 ICP-MS following procedures outlined in Reiners (2005). The closure temperatures is 160-200°C for zircon grains and 55-88°C for apatite grains (Farley, 2000; Reiners et al., 2004; Reiners et al., 2005). Analyzed thermochronological data were processed and reduced following the procedure from University of Michigan to obtain (U-Th)/He ages of both zircon and apatite. In order to arrive at an age the following equation was utilized:

$$^4\text{He} = 8 \cdot {}^{238}\text{U} \cdot (e^{\lambda_{238}t} - 1) + 7 \cdot {}^{235}\text{U} \cdot (e^{\lambda_{235}t} - 1) + 6 \cdot {}^{232}\text{Th} \cdot (e^{\lambda_{232}t} - 1) + 1$$

$$\cdot {}^{147}\text{U} \cdot (e^{\lambda_{147}t} - 1)$$

with decay constants $\lambda_{238} = 1.55125 \times 10^{-10}$year^{-1}, $\lambda_{235} = 9.8485 \times 10^{-10}$year^{-1}, $\lambda_{232} = 4.948 \times 10^{-11}$year^{-1}, and $\lambda_{147} = 6.539 \times 10^{-12}$year^{-1}; t is the elapsed time in years since the system closed, and ^{4}He, ^{238}U, ^{235}U, ^{232}Th, and ^{147}Sm are the amounts in moles (Zeitler, 2014). This equation cannot be solved algebraically (Zeitler, 2014). An iterative technique known as the Newton-Raphson method was used to obtain a solution once sufficient iterations are made (Zeitler, 2014). Time-temperature (t-T) paths were modeled using QTQt inverse modeling software (Gallagher et al., 2009).

3.4 - Inverse Thermal Modeling

To constrain the history and magnitude of uplift, we attempted to document the cooling history of the area associated with vertical uplift during transpressive deformation. We utilized (U-Th)/He thermochronological analysis on zircon and apatite grains to determine the age at which a given rock sample cooled below the closure temperature for the selected mineral. Low temperature thermochronology is an important method used to constrain the time-temperature history of rocks and provides constraints on the thermal history of geologic terrains (Gallagher et al., 2005). Within this software the data obtained through the (U-Th)/He thermochronology, including kinetics for any mineral/isotope system (in our case U, Th, He, Sm for apatite grains and U, Th, He for zircon grains) can be input. The shape of the crystal is another important parameter (meaning euhedral, subhedral, or otherwise). The model used in this study allows for multiple sample modeling, if the samples being used have the same form of thermal history (i.e. they can be treated as a vertical profile) (Gallagher et al., 2005). The vertical profile sampling strategy aims to utilize the spatial link between the samples vertically, rather than horizontally (Gallagher et al., 2005). By doing this, each sample is considered to have experienced the same thermal history, with the assumption that the lower elevation samples are always hotter than the higher elevation samples (Gallagher et al., 2005). This assumption comes from the idea that the lower elevation samples were deeper in the crust prior to erosion, and the higher elevation samples were shallower in the crust (Gallagher et al., 2005). One issue with these age-elevation profiles is that they are often not perfectly vertical and there may be situations where local fault movement or fluid flow will make these assumptions invalid (Gallagher et al., 2005). However, according to Gallagher et al. (2005) if these factors are significant, they should be apparent in the data.

Once all data is input into the program, QTQt uses an inversion scheme known as the

Bayesian transdimensional Markov chain Monte Carlo (MCMC) method, which model He diffusion in samples (Gallagher et al., 2013). The thermal history solutions are inferred from the data rather than being specified in the program (like is done in forward modeling) (Gallagher et al., 2013). The MCMC method allows a wide range of possible thermal histories to be considered as general information on time and temperature (Gallagher et al., 2013). One of the reasons the vertical profile method is more widely used (and why we used it in this study) is because it also allows temperature offset to be considered alongside time and temperature (Gallagher et al., 2013). QTQt allows for more focused geological constrains to be incorporated in the program to further focus the model (Gallagher et al., 2013). This can include depositional age and temperature among other time temperature constrains. The Bayesian approach naturally prefers simpler thermal history models and thus reduces any problems associated with over interpretation of inferred thermal histories (Gallagher et al., 2013). The output of this method is an assemblage of thermal histories, which provides importance to the range of accepted models in terms of a subsequent probability distribution (Gallagher et al., 2013). There are a variety of individual models that can be examined, including the best fitting data (maximum likelihood) model and the expected model (the weighted mean from the subsequent distribution) (Gallagher et al., 2013).

Within the QTQt program we designated a series of parameters based on known geological data within our study area. The rocks within our study area were deposited in the late Jurassic to late Cretaceous and being sedimentary rocks, were deposited at the surface (Bailey et al., 1970; Jayko et al. 1987; Hall, 1991; Graymer et al., 2014; Chapman et al., 2016). This allows us to input a depositional age for each sample with a time of 140 ± 40 Ma and a temperature of 10 ± 9.99 °C. Using the thermal model QTQt allowed us to specify one general time-temperature box, from which time-temperature points are sampled to construct a continuous thermal history

by linear interpolation between samples points. This method allows for up to five additional time-temperature boxes to be specified to allow us to add more specific constraints on the thermal history (Gallagher et al., 2009). With evidence of the post-metamorphic thermal anomaly, we specified that the rocks had to have undergone a heating event after being deposited and metamorphosed. Depending on which temperature zone the rocks were in, we specified this by designating an additional time temperature box with a time of 50 ± 40 Ma. We designated a temperature of 240 ± 30 °C for the NB19-032 and NB19-015 (Figure 3.1) run and a temperature of 210 ± 30 °C for the run of Steely's (2016) data within the Salmon Creek and NB19-021. By using the thermal model (QTQt) to compute the best thermal path for each analyzed sample, an estimated uplift rate for the Nacimiento block can be determined. By doing this process we can determine whether the Nacimiento block was affected by a hydrothermal event or by differential uplift.

Chapter 4 - Results

4.1 - Structural analysis

Results of regional structural mapping and structural analysis of the Nacimiento block are summarized in Figure 4.1. Structural analysis based on satellite image demonstrates that the regional fabrics, such as bedding (S_0), are oriented N315°-N350° (Figure 4.1). This orientation is in agreement with structural data published in Graymer et al. (2014) and is related to the eastward subduction of the Farallon plate below the North American plate and the imbrication of westward thrust sheets, associated folds and axial plane foliation (Cole and Basu, 1995; Underwood et al., 1999; Graymer et al., 2014). In contrast, within the thermal anomaly the regional structure orientations highlighted on satellite images appear different. This is also supported by our structural analyses performed in the field, which suggest E-W trending structures (S_0, fold, foliation, etc.), significantly contrasting with the regional fabrics (Figure 4.1). This drastic orientation change suggests a counterclockwise rotation of about 50°- 75° compared to the regional fabrics. We infer that the observed rotation of the regional fabrics along the regional thermal anomaly highlights the presence of a transpressional uplift developed between the San Gregorio Hozgri Fault (SGHF) and the Nacimiento Fault during dextral movement (Hughes, 2018; Lacroix et al., 2020). This would explain the exposure of previously deeply buried and consequently warmer rocks along this apparent thermal anomaly.
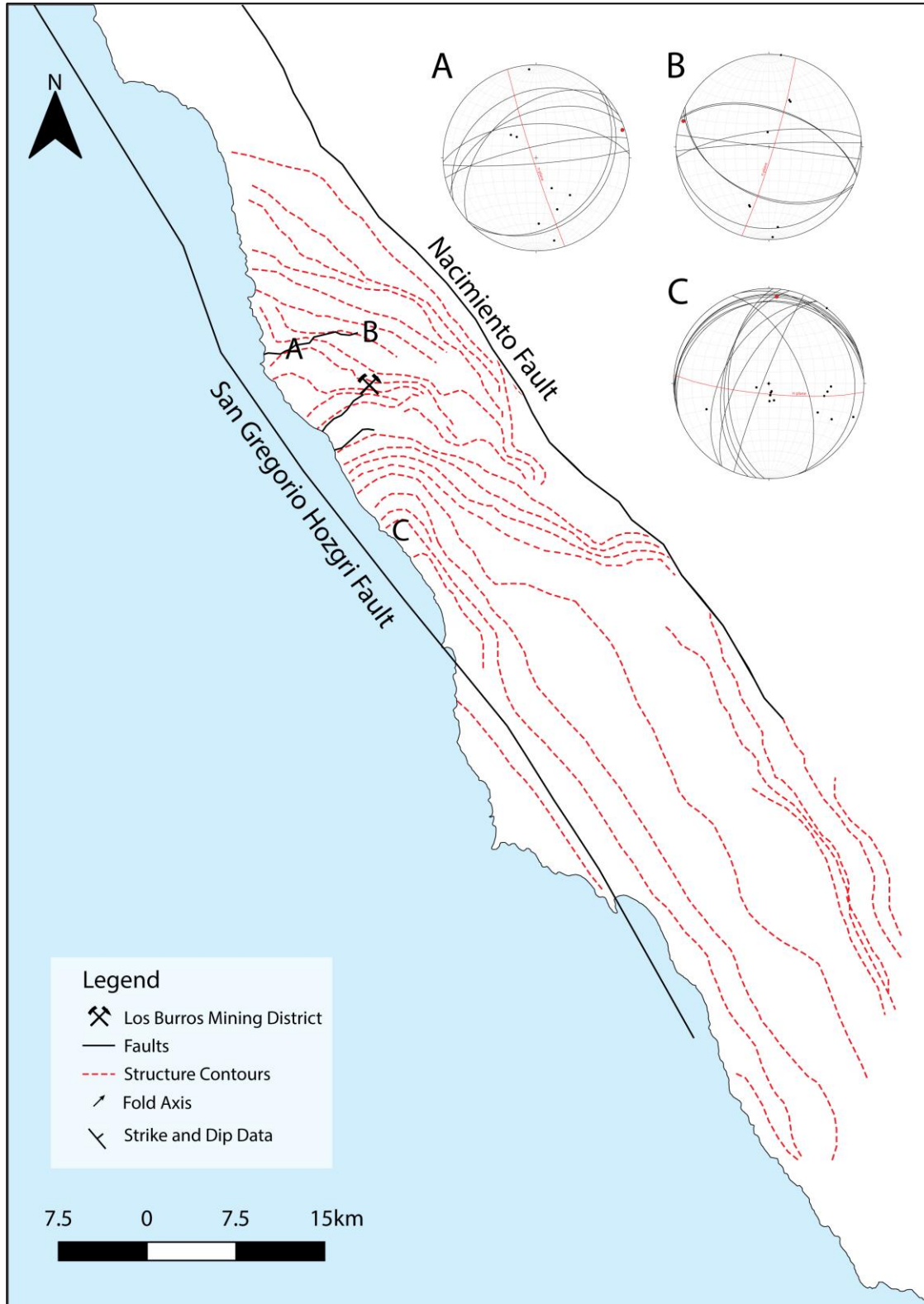
Figure 4.1 Map showing compiled structural data from fieldwork and Graymer et al. (2014) with interpreted structure contours in red. Stereonets detail fold analyses done on various folds in the Nacimiento block.

4.2 - RSCM Results

The Nacimiento block has been studied extensively using the RSCM technique by Lahfid et al. (in prep), but this work focused on a regional scale perspective. In order to better constrain the local post-subduction peak temperature distribution and the effect of small magmatic intrusions observed within the thermal anomaly on the maximum temperatures recorded by metasediments, samples were collected near the center of the thermal anomaly close to a small igneous intrusion (Figure 4.2). Four samples were collected near the igneous intrusion; sample A being the closest and sample D being the furthest away. Sample A was collected ~5 ft from the intrusion, sample B was collected ~12 ft from the intrusion, sample C was collected ~24 ft from the intrusion, and sample D was collected ~48 ft from the intrusion (Figure 4.2). Sample A gave a temperature of 227 ±27.8, sample B gave a temperature of 249 ±29.9, sample C gave a temperature of 241 ±28.9, and sample D gave a temperature of 240 ±18.1. The temperatures calculated by RSCM (i.e. T_{RSCM}) overlap within analytical uncertainty and suggest that there is no systematic increase in T_{RSCM} toward the intrusion suggesting 1) the thermal conditions of the surrounding rocks at the time of the magmatic intrusion were already high temperatures, 2) the intrusion cooled too fast to form the carbonization needed for RSCM, 3) the intrusion is small, so there could be a larger intrusion underneath the earths surface that could be causing this apparent thermal anomaly, or 4) there is no connection between magmatic intrusions and the regional thermal anomaly. Something to note is that the T_{RSCM} is very low for this type of contact metamorphism. However, further studies need to be completed to further investigate this point.
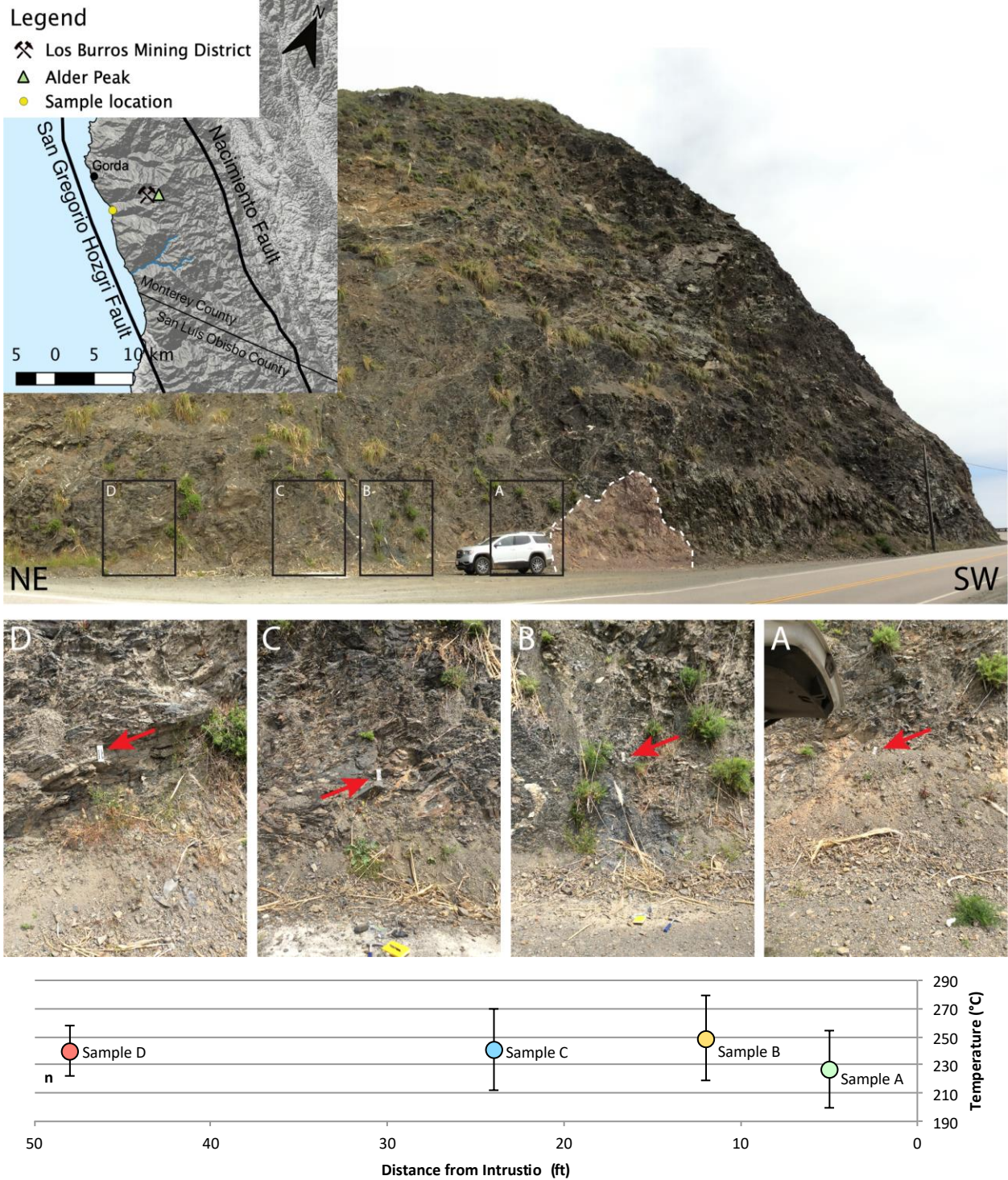
Figure 4.2 Location where RSCM samples were collected. Dashed area indicates the igneous intrusion that is the frame of reference for sample collection distances. White rectangle, indicated by red arrow, in each inset picture shows location of where the carbonaceous metasediment was collected.

4.3 - Thermochronological analysis

The data gathered from thermochronological analysis can be used to identify whether the study area has been affected by a hydrothermal event or by differential uplift. A summary table of thermochronological results is shown in Table 4.1 and a figure of sample locations and ages is shown in Figure 4.3.

Thermochronological results show a distinct younging trend toward the center of the thermal anomaly (Figure 4.4). These results show an age of 3.87 ± 0.28 Ma from sample NB19-032 near the center of the thermal anomaly from the apatite grains and 11.77 ± 2.00 Ma from sample NB19-004 at the center of the thermal anomaly from the zircon grains. The ages increase the further from the center of the thermal anomaly one gets (Figure 4.3). The furthest sample from the thermal anomaly (Sample NB19-025) has an age of 8.10 ± 1.60 from apatite and 85.13 ± 13.09 Ma from zircon. The zircon age is similar to the U-Pb detrital geochronology on detrital zircons, done by Chapman et al. (2016), which determined deposition within the Nacimiento block was estimated to have taken place 95 to 82 Ma. Sample NB19-004 at the center of the thermal anomaly did not have any apatite grains to be age dated. In fact, none of the samples that were collected from this area with a temperature above 290 °C had any apatite grains.

Table 4.1 Summary of low temperature thermochronological ages. For complete data set see Appendix A.

Map ID/ Sample #	Latitude/Longitude	Elevation (m)	No. of aliquots	Cooling age ± 1σ
Apatite (U-Th)/He				
NB19-015	35.8811, -121.371	1057	3	5.95 ±0.17
NB19-019	35.8646, -121.339	935	3	6.41 ±0.87
NB19-021	35.8472, -121.276	781	4	6.34 ±0.33
NB19-025	35.6142, -121.071	59	4	8.10 ±1.60
NB19-032	35.8579, -121.415	30	4	3.87 ±0.28
Zircon (U-Th)/He				
NB19-004	35.8847, -121.414	810	3	11.77 ±2.00
NB19-015	35.8811, -121.371	1057	3	32.84 ±8.92
NB19-019	35.8646, -121.339	935	3	21.19 ±2.63
NB19-021	35.8472, -121.276	781	3	78.15 ±19.77
NB19-025	35.6142, -121.071	59	3	85.13 ±13.09
NB19-032	35.8579, -121.415	30	3	13.75 ±2.57
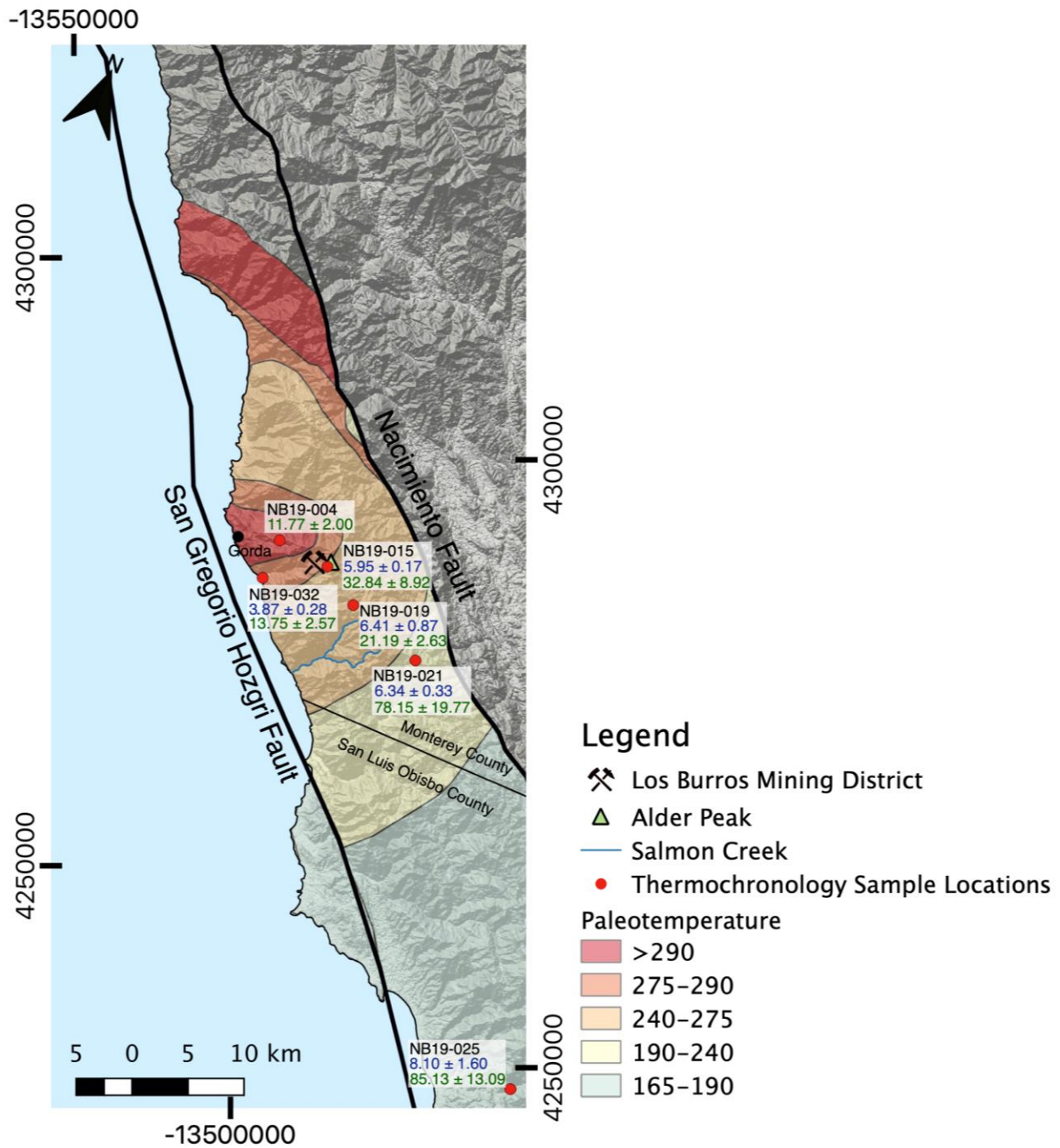
Figure 4.3 Thermochronology sample locations and results showing a younging trend towards the center of the thermal anomaly by sample NB19-004 to the outskirts shown by sample NB19-025. Apatite data indicated in blue and zircon data indicated in green.
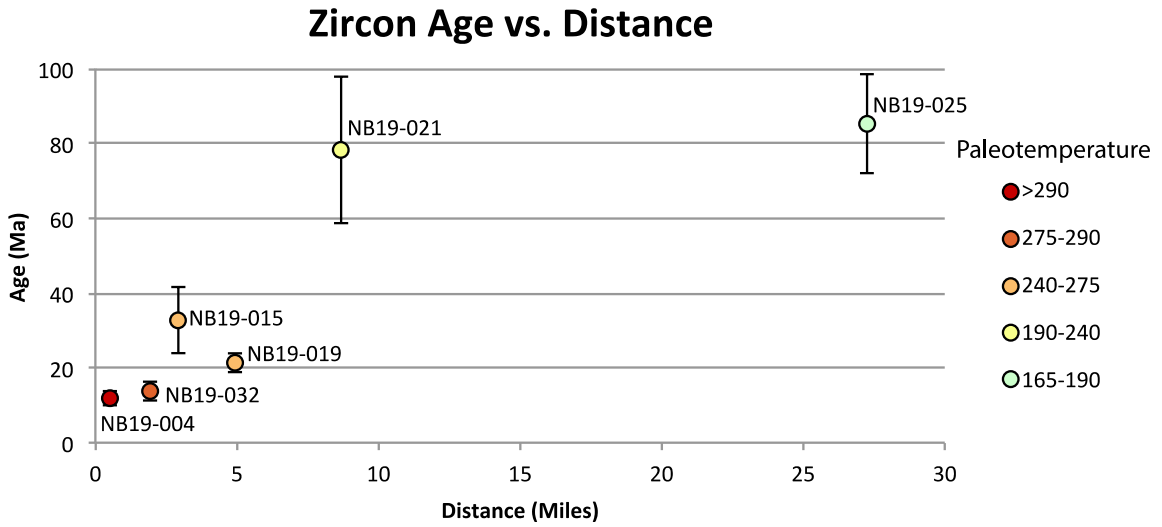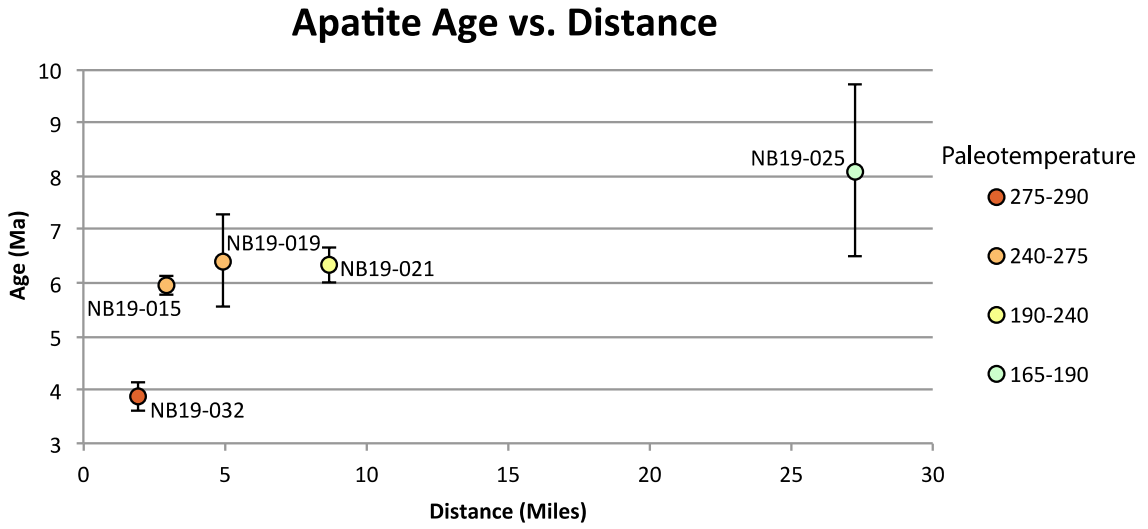
Figure 4.4 Graphs showing age in Ma vs. Distance in miles of the samples across the thermal anomaly temperature gradient. Distance is approximated from the center of the thermal anomaly. Error of age is also shown for each sample.

Chapter 5 - Discussion

5.1 - Link between structures and thermal anomaly

The Nacimiento block has a complex geologic and tectonic history. One of the major features affecting the area is the hypothesized post-metamorphic thermal anomaly. However, it is still unclear whether the post-subduction thermal anomaly is a response to hydrothermal processes or to rapid vertical uplift by transpressive deformation.

The regional structural analysis completed as part of this study has been combined with the RSCM thermometry of 50 samples from the Nacimiento block completed by Lahfid et al. (in prep) to produce a new peak-temperature distribution map (Figure 3.1, Figure 4.4, and Figure 5.1). The RSCM map shows the presence of a significant thermal anomaly (up to 340°C) in the vicinity of Cape San Martin/Los Burros (Figure 5.1). These findings are in agreement with the post-subduction thermal anomaly proposed by Underwood et al. (1995) and Underwood and Laughland (2001) based on vitrinite reflectance and illite crystallinity measurements on Franciscan metasediments. However, the shape of the thermal anomaly on their paleotemperature map could only be inferred inland, because they only gathered data along the coastline (Underwood et al., 1995). Our new RSCM temperature distribution map suggests that the LBMD is not in the center of the thermal anomaly, as suggested by Underwood and Laughland (2001), but rather at the edge of it (Figure 5.1). Interestingly, the reorientation of the structures is spatially correlated with the thermal anomaly (Figure 5.2). Also, the orientation of the temperature contours crosscut the metamorphic isograds from Ernst (1980) (Figure 5.3), suggesting that this high temperature anomaly is post-subduction. In addition, the northern and southern edges of the highest (>290°C) temperature contour from the thermal anomaly seem to be bound by two major E-W valley incisions that have been recently interpreted by Graymer et al. (2014) as major reverse faults (Figure 5.2).

The clear spatial correlation that exists between the post-subduction thermal anomaly and E-W structural orientation could be explained by: 1) the presence of a transpressive ridge that would expose deeper and thus warmer rocks to the surface; 2) the presence of hydrothermal and/or magmatic activities, or 3) the combination of both.

Our first hypothesis is well supported by structural data. Deformation in this area shows a counterclockwise rotation from the regional fabrics oriented N315°-N350° (Lacroix et al., 2020). This rotation of about 50°- 75° compared to the regional fabrics supports the hypothesis of transpressive deformation. The two faults that bound the thermal anomaly are likely reverse faults, which would accommodate significant vertical uplift. Transpressive deformation is common along strike-slip faults and is very common in California (Dewey et al., 1998; Spotila et al., 2001). In addition, similar rotational deformation has been described by Sorlien et al. (1999) for an offshore section of the SGHF just south of our study area. However, with the center of the thermal anomaly at about 350°C compared to the temperature background at 250°C, and assuming a normal geothermal gradient of about 30°C/km (Bostick et al., 1978; Niemi and Clark, 2018), this would require an uplift of rock buried at more than 3km below the surface. For this model to be plausible, the rocks at the surface of the thermal anomaly would be older than the rocks outside of the thermal anomaly due to the uplift of the older rocks below. However, the rocks exposed to the surface in both the thermal anomaly and outside of it, consist of metasediments from the late Jurassic to early Cretaceous Franciscan group (Bailey et al., 1970; Jayko et al. 1987; Hall, 1991; Graymer et al., 2014; Chapman et al., 2016), which does not support this model.

The second hypothesis would require hydrothermal fluid flow and magmatism. However, Hughes (2018) found that the fluid inclusions within the LBMD were characterized by low salinity, low CO_2 content, and did not show evidence for fluid boiling, which is not consistent

38

with a hydrothermal (e.g. fluid heated by magmatic body) source. In contrast, based on oxygen stable isotope composition of Au-bearing veins, Lacroix et al. (2020) suggest that the LBMD gold deposits source fluid is likely derived from the metamorphic dewatering of organic-rich sediments. Hughes (2018) found that the P-T conditions of the mineralization of the LBMD are 300°C ±20°C with a pressure of ~800 bars, based on fluid inclusion data. It is worth noting that this range of temperatures is lower than the local RSCM temperatures (>360°C) recorded in the area. Such findings strongly contrast with the hypothesis of Underwood et al. (1995), who suggest that the thermal anomaly is mainly caused by a hydrothermal event caused by emplacement of the Los Burros ore deposit. These P-T conditions represent the hydrostatic 30°C/km geothermal gradient. In addition, through the use of RSCM, we have found that the magmatic intrusions do not have a strong effect on the RSCM temperatures of the surrounding host rock (Figure 4.2). Collectively, these observations do not support the formation of the post-metamorphic thermal anomaly by hydrothermal processes alone, because 1) the derivation of the fluid inclusions within the LBMD are not consistent with a magmatic source (Lacroix et al., 2020), 2) the LBMD formed at temperatures lower than the peak temperatures recorded by host rocks, and 3) the RSCM temperatures of the metasediments in the area do not seem to be affected by the magmatic intrusions.

In this study we prefer the third hypothesis, which corresponds to a combination of transpressive deformation and hydrothermal activity. First, this hypothesis is well supported by clear evidence of transpressive deformation, which would uplift warmer rocks (Lacroix et al., 2020). This is supported by the rotation of the regional structures, and the presence of Au-mineralization associated with the formation of "en-echelon" veins, which are both indicative of a transpressive event (Lacroix et al., 2020). In addition, numerous quartz-carbonate veins and veinlets are observed along the RSCM thermal anomaly, suggesting fluid-flow during the

transpressional deformation (Figure 5.4) (Lacroix et al., 2020). The potential for hydrothermal processes to have contributed to the anomaly is clearly supported by the presence of a magmatic intrusion in the area (Dickinson and Snyder, 1979; Dickinson, 1997), associated country rocks with elevated temperatures in the vicinity of the intrusion, and the fluid flow within the veins of the Los Burros Au deposit (Lacroix et al., 2020).

However, the model proposed above is only based on structural observations and temperature distribution. It lacks age constraints. Therefore, in the next section we discuss the results of our low-temperature (U-Th)/He thermochronmetry analyses on apatite and zircon grains in order to better understand the timing of vertical transpressional uplift and the associated LBMD emplacement.
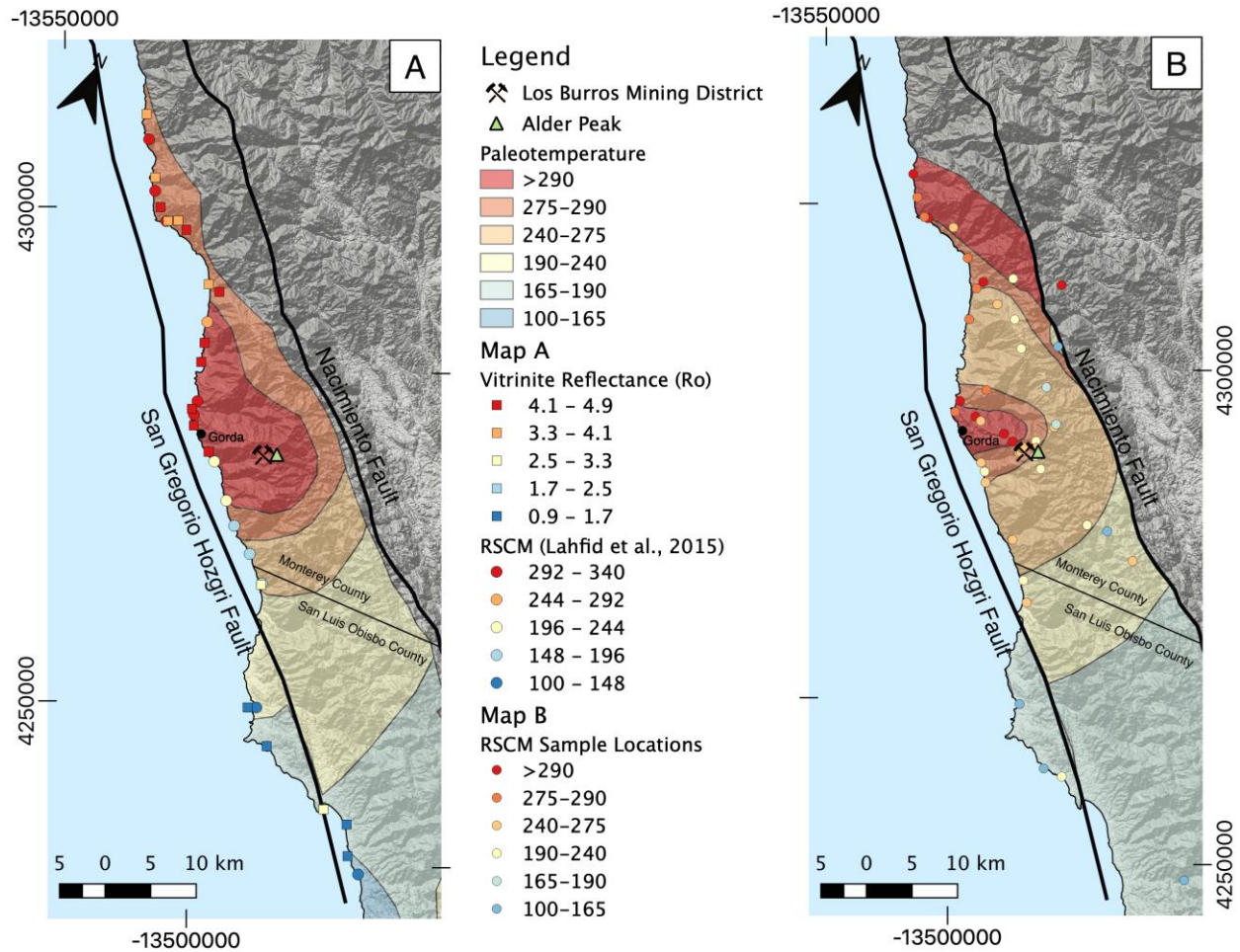
Figure 5.1 Comparison of previously interpreted thermal anomaly by Underwood and Laughland (2001) vs. our new proposed peak temperature map. A) Map of Underwood et al. (1995) Ro data vs. Lahfid et al. (2015) RSCM data. Thermal maturity pattern for Franciscan rocks of the central California coast proposed by Underwood et al. (1995). *Figure modified from Underwood and Laughland (2001).* B) New proposed peak temperature map of the Nacimiento block thermal anomaly. Data indicated by dots are from Lahfid et al. (in prep).
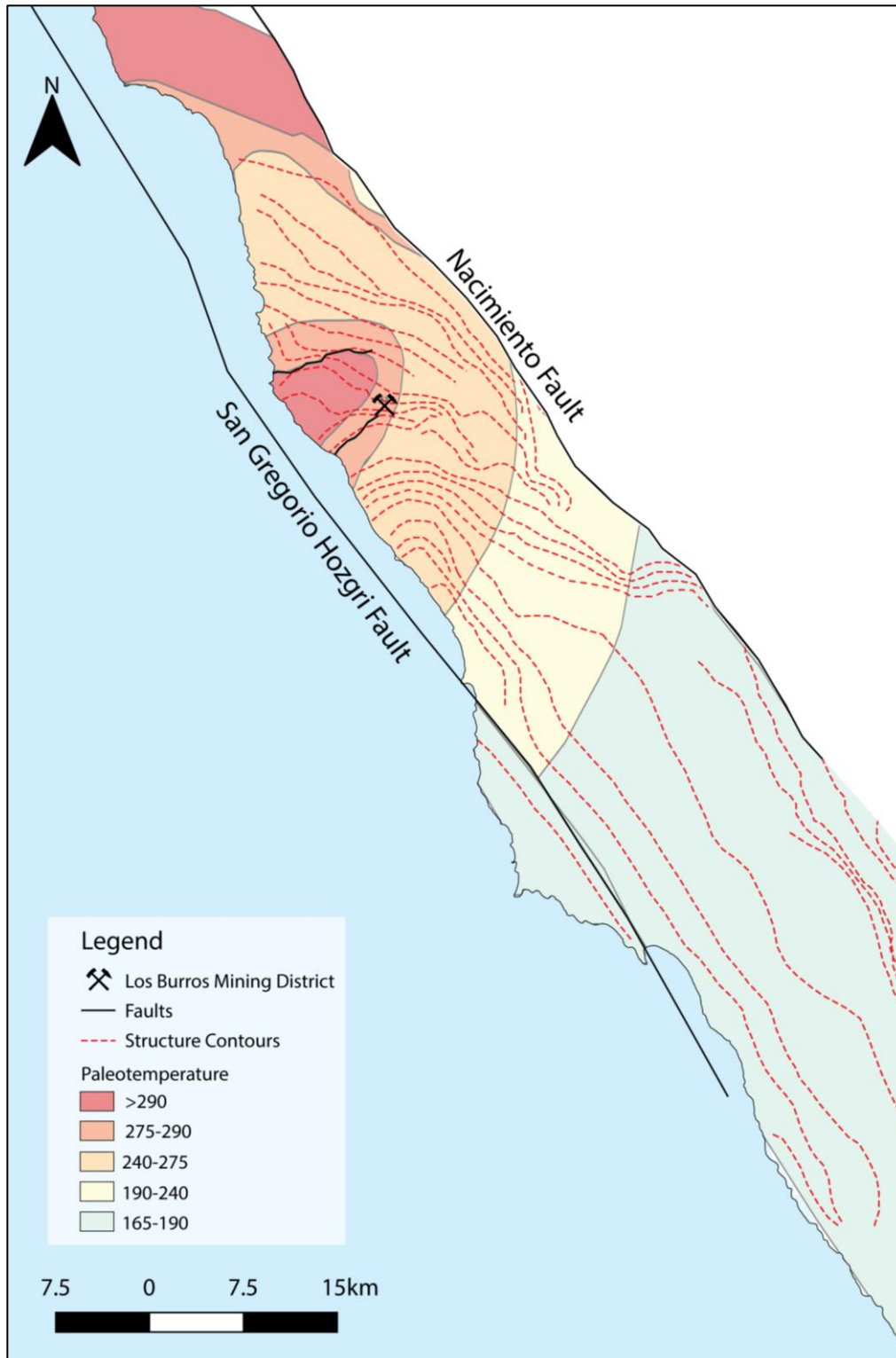
Figure 5.2 Map showing new proposed peak temperature map of the Nacimiento block thermal anomaly with interpreted structure contours to show relationship between structural reorientation and the thermal anomaly. *Thermal anomaly data used for interpretation from Lahfid. Structural data used for interpretation from fieldwork as part of this thesis project and Graymer et al. (2014).*
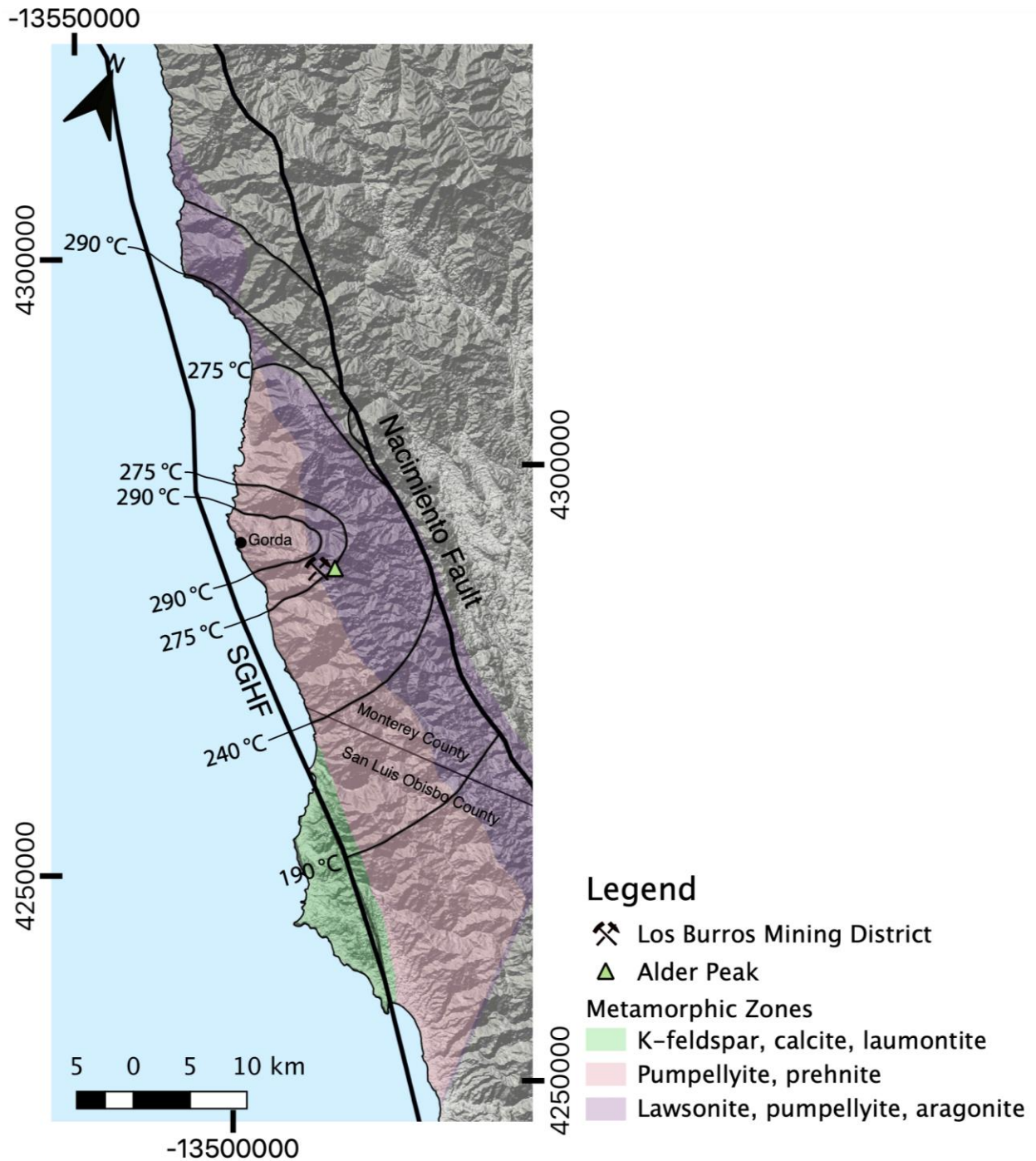
Figure 5.3 Map showing the comparison of the Franciscan metamorphic zones from Ernst (1980) vs. our new proposed peak temperature map of the Nacimiento block thermal anomaly to show the orientation of the temperature contours crosscut the metamorphic isograds. *Figure modified from Underwood et al. (1995).*
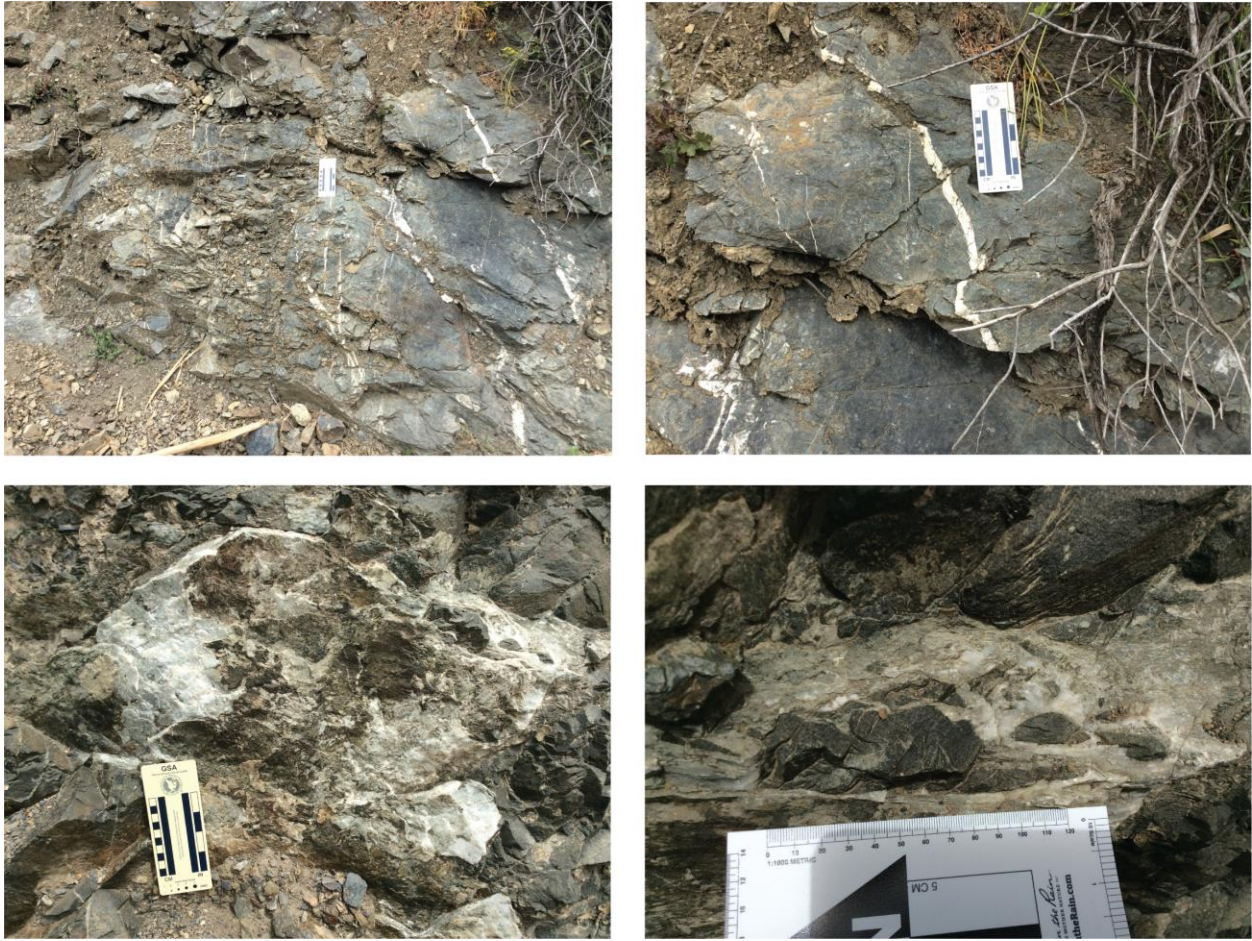
Figure 5.4 Pictures showing a variety of veins located within the vicinity of the LBMD.

5.2 - Thermochronological analysis interpretation

(U-Th)/He thermochronometry results obtained on both apatite and zircon grains show a distinct younging trend toward the center of the thermal anomaly (Figure 4.3). With one exception (Sample NB19-032), the youngest (U-Th)/He ages are recorded in rock samples collected at a higher elevation (Figure 5.5). Sample NB19-032 was collected along a road cut/fault zone, making the elevation of this sample incomparable to the rest. These two observations strongly suggest the uplift of younger and warmer rocks along the RSCM thermal anomaly, which supports our hypothesis of vertical uplift in the area.

In order to better constrain the thermal history of the Nacimiento block, particularly within the LBMD-Cape San Martin area, we have integrated our (U-Th)/He ages with a thermal model using QTQt software (Gallagher et al., 2009). QTQt uses an inversion scheme known as the Bayesian transdimensional Markov chain Monte Carlo (MCMC) method, which model He diffusion in samples (Gallagher et al., 2013) Through this modeling method, the program is able to infer the statistically most likely thermal path. In order to better constrain this model we input known geologic data from within our study area. The rocks within our study area were deposited in the late Jurassic to late Cretaceous and being sedimentary rocks, were deposited at the surface (Bailey et al., 1970; Jayko et al. 1987; Hall, 1991; Graymer et al., 2014; Chapman et al., 2016). This allows us to input a depositional age for each sample with a time of 140 ± 40 Ma and a temperature of 10 ± 9.99 °C. In addition to this, depending on which temperature zone the rock samples were in, we specified this by designating an additional time temperature box with a time of 50 ± 40 Ma. We designated a temperature of 240 ± 30 °C for the NB19-032 and NB19-015 (Figure 4.3) run and a temperature of 210 ± 30 °C for the run of Steely's (2016) data within the Salmon Creek and NB19-021. The results from this inverse thermal model of the preferred thermal history are shown in Figure 5.6 and Figure 5.7. The calculations suggest that the primary

depositional age is between 170 – 120 Ma, which is in agreement with previous studies that reported late Jurassic to early Cretaceous ages for the rocks within the Nacimiento block (Bailey et al., 1970; Jayko et al. 1987; Hall, 1991; Graymer et al., 2014; Chapman et al., 2016). Deposition is followed by rapid burial and subsequent high-pressure, low-temperature metamorphism conditions between 125 and 90 Ma, which is in agreement with the hypothesis of Suppe and Armstrong (1972) and Ernst (1980) suggesting that metamorphism occurred soon after deposition. Around 20 – 25 Ma, the thermal history is affected by a large temperature peak followed by rapid uplift (Figure 5.6 and Figure 5.7). We infer that this large temperature peak is related the subduction of a spreading center (Dickinson and Snyder, 1979). With the subduction of a triple junction, this allows for a slab-free region to develop beneath the continent where no subducted slab is present (Dickinson and Snyder, 1979). This allows for the upwelling of the sub-slab mantle, which could in turn generate a high temperature thermal overprint on the metasediments and changes in the regional geodynamics. In the following we will discuss the effects of such triple-point subduction on the Nacimiento block.

Apatite Elevation vs. Age

Zircon Elevation vs. Age
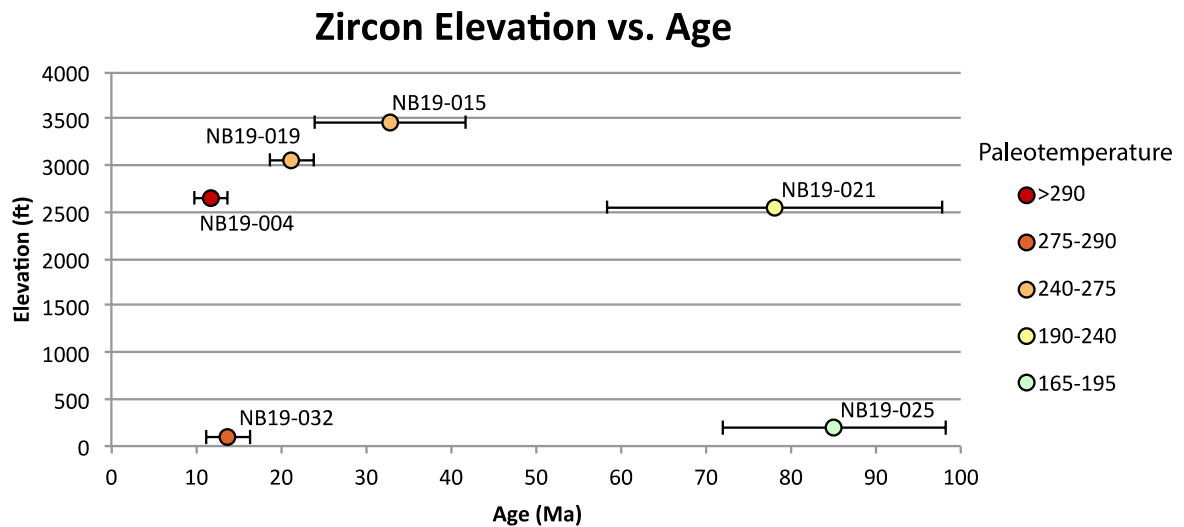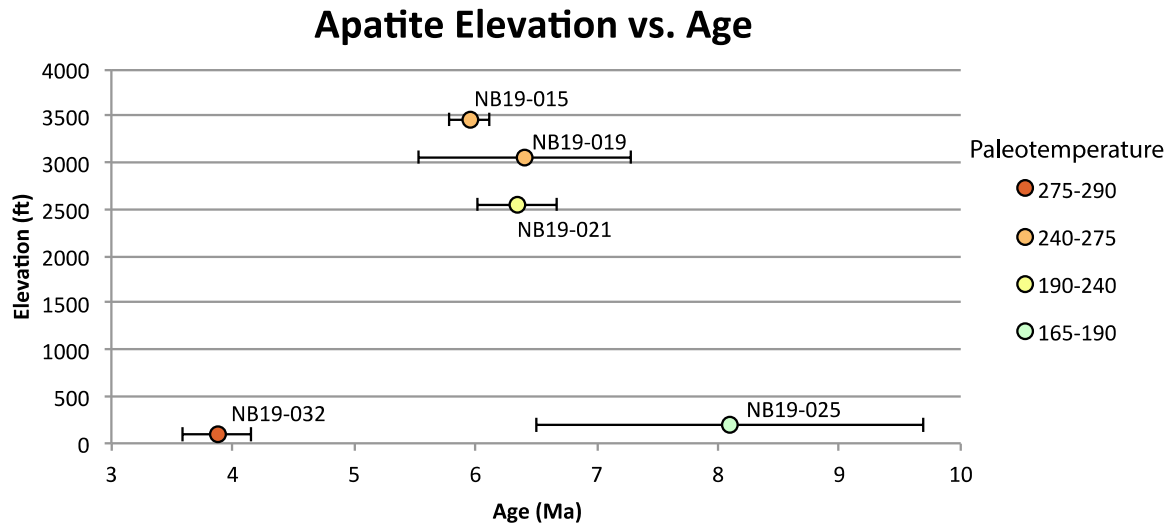
Figure 5.5 Graphs showing elevation in feet vs. age in Ma of the samples across the thermal anomaly temperature gradient. Sample NB19-032 was collected near a fault zone along a road-cut and therefore has a lower elevation than its counterparts on either side. Error of age is also shown for each sample.
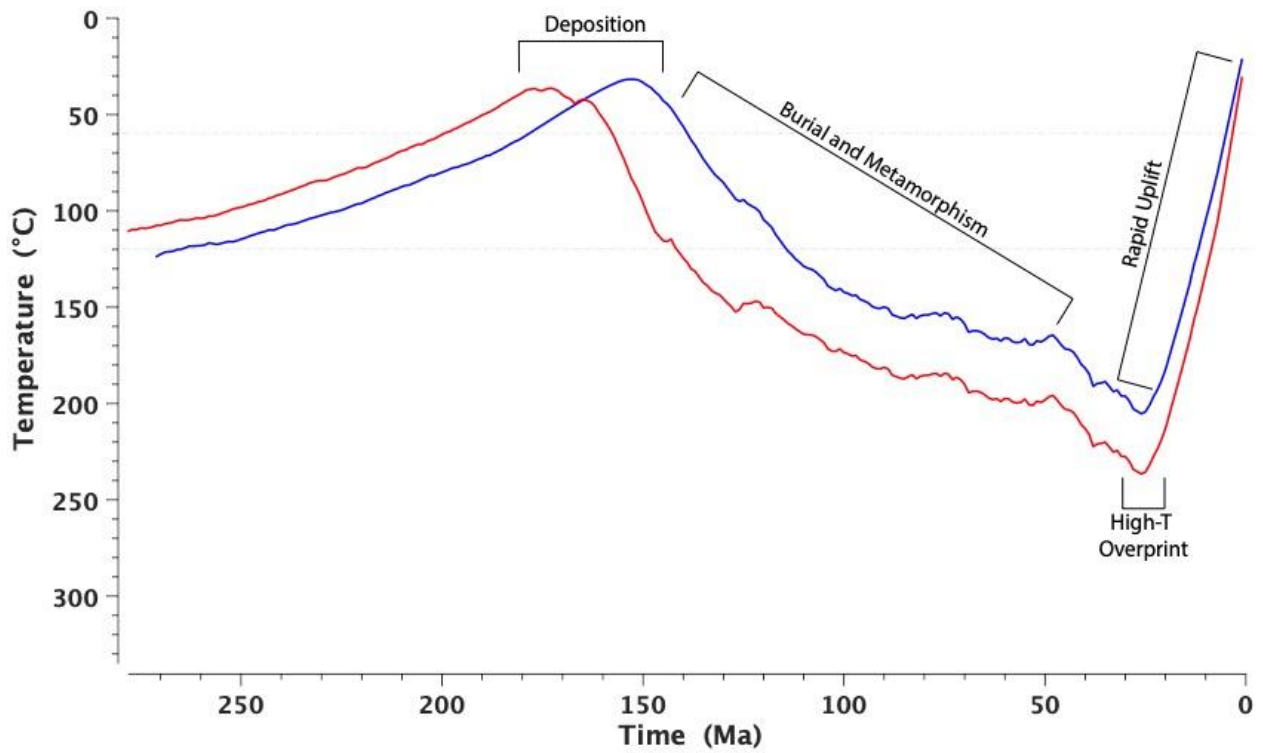
Figure 5.6 Inverse thermal model of preferred thermal history of NB19-015 and NB19-032. The blue line is the stratigraphic high (sample NB19-015) and the red line is the stratigraphic low (sample NB19-032).
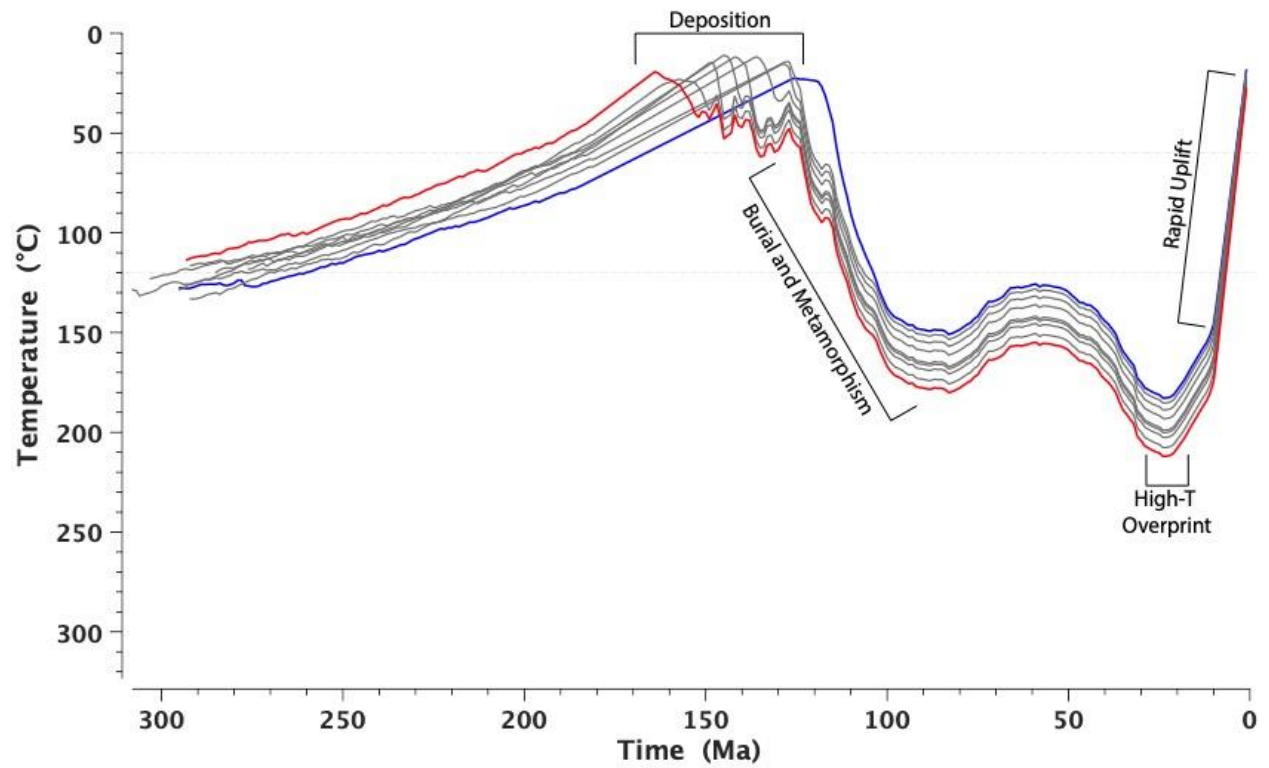
Figure 5.7 Inverse thermal model of preferred thermal history of Salmon Creek data from Steely (2016) data and NB19-021. The blue line is the stratigraphic high (sample AS026), the red line is the stratigraphic low (sample AS047), and the grey lines are intermediate.

5.3 – Geodynamics of the Nacimiento Block

Subduction of an oceanic spreading center disrupts the overriding plate both thermally and mechanically (e.g., Delong and Fox, 1977) (Haeussler et al., 2003). The two diverging oceanic plates will continue to separate even after they are subducted and new oceanic crust is no longer formed in the gap between them (e.g., Thorkelson, 1996) (Haeussler et al., 2003). The overriding plate comes in contact with hot, upwelling asthenosphere and results in anomalous igneous and hydrothermal activity (Dickinson and Snyder, 1979; Haeussler et al., 2003). In general, the subducting ridge is neither parallel nor perpendicular to the subduction zone. With the subduction of an oceanic spreading center (triple junction) there are four geologic features that appear: 1) plutons, 2) high-temperature, low-pressure metamorphic conditions, 3) dikes, and 4) gold-quartz mineralized veins (Haeussler et al., 2003).

Dickinson and Snyder (1979) hypothesize that there was a triple junction formation in the Nacimiento block and surrounding area sometime in the early Neogene. They suggest that the formation of the San Andreas Fault strike-slip system reflects the subduction of an oceanic spreading center into the mantle beneath western North America (Dickinson and Snyder, 1979; Dickinson, 1997). This allowed for a slab-free region to develop beneath the continent where no subducted slab is present adjacent to the transform fault (Dickinson and Snyder, 1979). Examples of this type of ridge subduction have been hypothesized in other areas worldwide (e.g., The Gulf of Alaska), which share similarities with the Cape San Martin-LBMD area.

In the Nacimiento block, there is clear evidence supporting the hypothesis of the subduction of a spreading center, similar to that observed in southern Alaska (Atwater, 1989; Sisson et al., 1989; Haeussler et al., 1995; Pavlis and Sisson, 1995; Kusky et al., 1997; Bradley et al. 2003). In southern Alaska there is an early Tertiary trench-ridge-trench convergent margin subduction zone (Sisson et al., 1989; Bradley et al. 2003). In this area there is widespread

subduction-generated magmatism in the Alaska Range, evidence of high temperature metamorphism that was superimposed onto the rocks; the latter took place after the regional low-grade metamorphic event and gold mineralization through hydrothermal systems (Haeussler et al., 1995; Bradley et al. 2003). Similarly, in the Nacimiento block, we observe magmatism associated with the subduction of the Mendocino triple junction, which is a fault-fault-trench subduction zone (Dickinson and Snyder, 1979; Dickinson, 1997), including a high-temperature, low-pressure post-subduction thermal overprint (Lahfid et al., 2015; Lahfid et al., (in prep)) and the Los Burros gold deposit, which consists of quartz-calcite-sulfide veins (Lacroix et al., 2020) (Figure 5.8). In southern Alaska, they observe ductile deformation (Pavlis and Sisson, 1995), strike slip and normal faults (Kusky et al., 1997), and an ~70-degree bend in magnetic anomaly pattern that implies that three oceanic plates once existed there, separated by three spreading ridges, which is suggested to have been caused by a triple junction (Atwater, 1989; Bradley et al. 2003). We observe a similar scenario in the Nacimiento block, where there is clear structure reorientation and 'en-echelon" veins (Lacroix et al., 2020) which further supports this hypothesis of a triple junction.
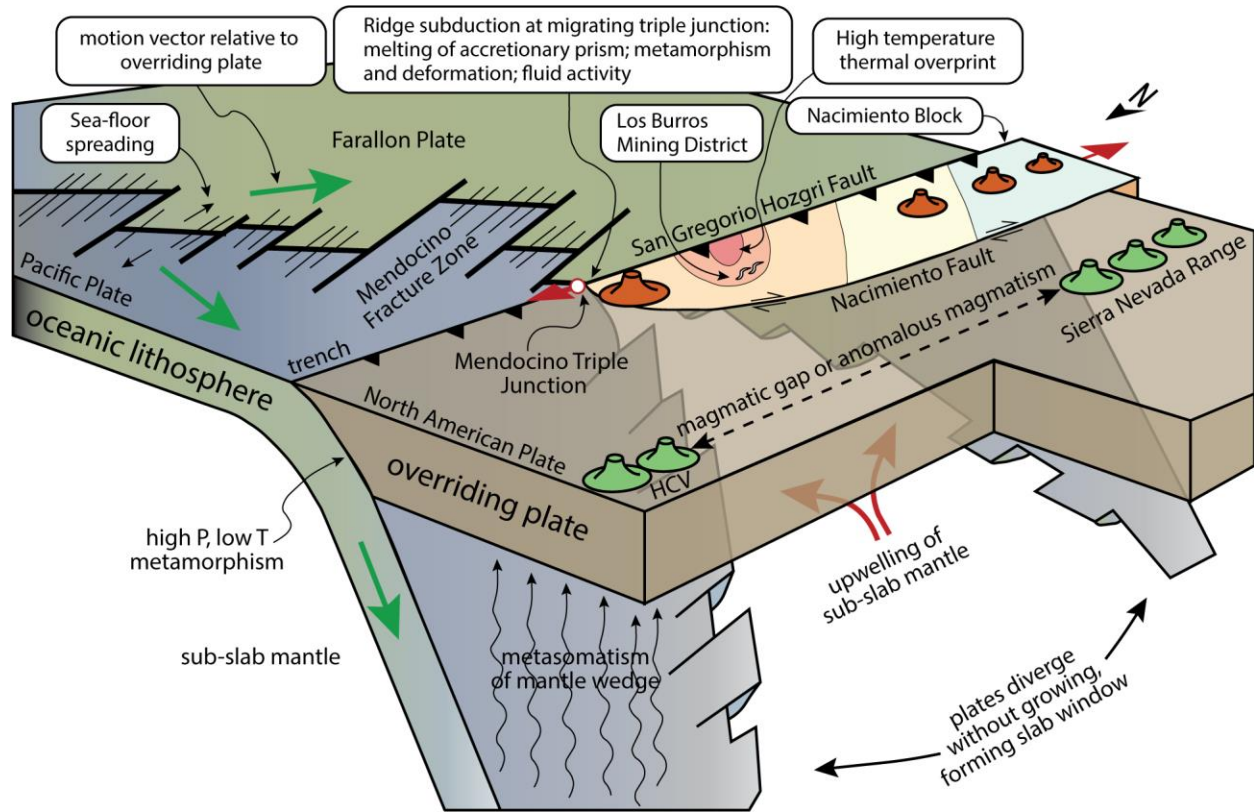
Figure 5.8 Thermal history model showing subduction of the paleo-Mendocino triple junction under the North American Plate during the Miocene. Orange cones indicate volcanoes. Green cones indicate volcanic fields/mountain ranges. HCV; High Cascade Volcanics. Figure modified from Thorkelson (1996), Sisson and Pavlis (1993), Sisson et al., (2003), Li et al. (2005), and Windley and Xiao (2018).

Chapter 6 - Conclusions

This work confirms the presence of a significant post-metamorphic thermal anomaly (up to 340˚C) in the vicinity of Cape San Martin/Los Burros, and inferred by Underwood and Laughland's (2001). The thermal anomaly is oriented E-W, which correlates with reorientation of regional subduction-related structures generally oriented N315°-N350°, near the center of the thermal anomaly. This orientation change suggests a counterclockwise rotation of about 50°- 75° compared to the regional fabrics. We infer that the observed rotation of the regional fabrics along the regional thermal anomaly highlights the presence of a transpressional uplift developed between the San Gregorio Hozgri Fault (SGHF) and the Nacimiento Fault during dextral movement. This could explain exposure of previously deeply buried and consequently warmer rocks along this apparent thermal anomaly.

Our low-temperature (U-Th)/He thermochronological analysis, performed on both apatite and zircon grains, shows a distinct younging trend toward the center of the thermal anomaly. In addition, with one exception, the younger rocks are at a higher elevation than the older rocks. Both observations are indicative of uplift of younger and warmer rocks.

Based on our QTQt modeling our results show a primary depositional age to be 170 – 120 Ma, followed by a rapid burial and high-pressure, low-temperature metamorphic conditions between 125 and 90 Ma, suggesting that metamorphism occurred soon after deposition. Finally, at around 20 – 25 Ma, we observe the thermal history is affected by a large temperature peak followed by rapid uplift. Based on these observations, we infer that this large temperature peak is related the subduction of a triple junction, similar to the trench-ridge-trench triple junction observed in southern Alaska.

In the Nacimiento block, there is clear evidence supporting the hypothesis of the subduction of a triple junction: (1) Magmatism associated with the subduction of the paleo-

Mendocino triple junction within the Nacimiento block and surrounding area (Dickinson and Snyder, 1979; Dickinson, 1997), (2) high-temperature, low-pressure post-subduction metamorphic conditions, (Lahfid et al., 2015; Lahfid et al., (in prep)), (3) a variety of dikes observed in the road cuts along HWY 1, and (4) the Los Burros gold deposit consisting of quartz-calcite-sulfide veins (Lacroix et al., 2020). The structure reorientation and the 'en-echelon" veins (Lacroix et al., 2020) observed in the Nacimiento block further supports this hypothesis. The evidence that we observe in the Nacimiento block is similar to areas in southern Alaska that have also undergone the subduction of a triple junction (Atwater, 1989; Sisson et al., 1989; Haeussler et al., 1995; Pavlis and Sisson, 1995; Kusky et al., 1997; Bradley et al. 2003).

References

Atwater, T., 1989, Plate tectonic history of the northeast Pacific and western North America, in Winterer, E.L., Hussong, D.M., and Decker, R.W., eds., The Eastern Pacific Ocean and Hawaii: Geology of North America, v. N, p. 21-72.

Bailey, E.H., Blake, M.C., and Jones, D.L., 1970, On-land Mesozoic oceanic crust in California Coast Ranges: U.S. Geological Survey Professional Paper 700-C, p. 70-81.

Beyssac, O., Goffé, B., Chopin, C., Rouzaud, J.N., 2002, Raman spectra of carbonaceous material in metasediments: A new geothermometer: Journal of Metamorphic Geology, v. 20, no. 9, p. 859-871

Bonal, L., Quirico, E., Bourot-Denise, M., and Montagnac, G., 2006, Determination of the petrologic type of CV3 chondrites by Raman spectroscopy of included organic matter: Geochimica et Cosmochimica Acta, v. 70, no. 7, p. 1849-1863.

Bostick, N.H., Cashman, S.M., McCulloh, T.H., and Waddell, C.T., 1978, Gradients of vitrinite reflectance and present temperature in the Los Angeles and Ventura basins, California, in Oltz, D.F., ed., Symposium in Geochemistry: Low Temperature Metamorphism of Kerogen and Clay Minerals: Los Angeles, Pacific Section of the Society of Economic Paleontology and Mineralogy, p. 65-96.

Bradley, D., Kusky, T., Haeussler, P., Goldfarb, R., Miller, M., Dumoulin, J., Nelson, S.W., and Karl, S., 2003, Geologic signature of early Tertiary ridge subduction in Alaska, in Sisson, V.B., Roeske, S.M., and Pavlis, T.L., eds., Geology of a transpressional orogen developed during ridge-trench interaction along the North Pacific margin: Boulder, Colorado, Geological Society of America Special Paper 371, p. 19-49

Burch, S.H., 1968. Tectonic emplacement of the Burro Mountain ultramafic body, Santa Lucia Range, California: Geological Society of America Bulletin 79, p. 527-544.

Buseck, P. R., and Beyssac, O., 2014, From Organic Matter to Graphite: Graphitization: Elements, v. 10, p. 421-426.

Chapman, A.D., Jacobson, C.E., Ernst, W.G., Grove, M., Dumitru, T., Hourigan, J., and Ducea, M.N., 2016, Assembling the world's type shallow subduction complex: Detrital zircon geochronologic constraints on the origin of the Nacimiento block, central California Coast Ranges: Geosphere, v. 12, p. 533-557.

Clark, J. C., 1998, Neotectonics of the San Gregorio fault zone: Age dating controls on the offset history slip rates: American Association of Petroleum Geologists Bulletin, v. 82, p. 884-885.

Cole, R.B., Basu, A.R., 1995, Nd-Sr isotopic geochemistry and tectonics of ridge subduction and middle Cenozoic volcanism in western California: Geological Society of America Bulletin 107, p. 167-179.

Cowan, D.S., and Page, B.M., 1975, Recycled Franciscan material in Franciscan mélange west of Paso Robles, California: Geological Society of America Bulletin, v. 86, p. 1089-1095.

Delong, S.E., and Fox, P.J., 1977, Geological consequences of ridge subduction, in Talwani, M., and Pitman, W.C., III, eds., Island arcs, deep sea trenches, and backarc basins: American Geophysical Union, Maurice Ewing Series, v. 1, p. 221–228.

Dewey, J.F., Holdsworth, R.E and Strachan, R.A., 1998, Transpression and transtension zones, in Continental Transpressional and Transtensional Tectonics, Holdsworth, R.E., Strachan R.A., and Dewey, J.F. eds., Geological Society Special Publication, n. 135, p. 1-14.

Dickinson, W.R., 1997, Tectonic implications of Cenozoic volcanism in coastal California: Geological Society of America Bulletin, v. 109, no. 8, p. 936-954.

Dickinson, W.R., and Snyder, W.S., 1979, Geometry of triple junctions related to San Andreas transform: Journal of Geophysical Research: Solid Earth, v. 84(B2), p. 561-572.

Ernst, W.G., 1980, Mineral paragenesis in Franciscan metagraywackes of the Nacimiento Block, a subduction complex of the Southern California Coast Ranges: Journal of Geophysical Research: Solid Earth, v. 85, no. B12, p. 7045-7055.

Ernst, W.G., 2015, Franciscan geologic history constrained by tectonic/olistostromal high-grade metamafic blocks in the iconic California Mesozoic-Cenozoic accretionary complex: American Mineralogist, v. 100, p. 6-13.

Farley, K.A., 2000, Helium diffusion from apatite: General behavior as illustrated by Durango fluorapatite: Journal of Geophysical Research, v. 105, no. B2, p. 2903-2914.

Gallagher, K., 2013, Transdimensional inverse thermal history modeling for quantitative Thermochronology: Geophysical Research Abstracts, v. 15.

Gallagher, K., Charvin, K., Nielsen, S., Sambridge, M., and Stephenson, J., 2009, Markov chain Monte Carlo (MCMC) sampling methods to determine optimal models, model resolution and model choice for Earth Science problems: Marine and Petroleum Geology, v. 26, no. 4, p. 525-535.

Gallagher, K., Stephenson, J., Brown R., Holmes, C., and Fitzgerald, P., 2005, Low temperature thermochronology and modeling strategies for multiple samples 1: Vertical profiles: Earth and Planetary Science Letters, v. 237, no. 1-2, p. 193-208.

Gibbons, H., Warrick, J., Ritchie, A., and Schmidt, K., 2017, USGS Monitors Huge Landslides on the California's Big Sur Coast, Shares Information with California Department of Transportation: U.S. Geological Survey.

Gilbert, W.G., 1973, Franciscan Rocks near Sur Fault Zone, Northern Santa Lucia Range, California: Geological Society of America Bulletin, v. 84, p. 3317-3328.

Graymer, R.W., Langenheim, V.E., Roberts, M.A., McDougall, K., 2014, Geological and geophysical maps of the eastern three-fourths of the Cambria 30'x 60'quadrangle, central

California Coast Ranges: US Geological Survey Scientific Investigations Map 3287, scale 1:100,000.

Haeussler, P.J., Bradley, D.C., Goldfarb, R., and Snee, L., 1995, Link between ridge subduction and gold mineralization in southern Alaska: Geology, v. 23, p. 995-998.

Haeussler, P.J., Bradley, D.C., and Goldfarb, R.J., 2003, Brittle deformation along the Gulf of Alaska margin in response to Paleocene-Eocene triple junction migration, in Sisson, V.B., Roeske, S.M., and Pavlis, T.L., eds., Geology of a transpressional orogen developed during ridge-trench interaction along the North Pacific margin: Boulder, Colorado: Geological Society of America Special Paper 371, p. 119-140.

Hall, C.A., 1991, Geology of the Point Sur–Lopez Point region, Coast Ranges, California: A part of the Southern California allochthon: Geological Society of America Special Paper 266, 40 p.

Hughes, J., 2018, Characterization and emplacement modeling of gold deposition within the Franciscan complex: An example from the Los Burros mining district, California [Master's thesis]: Manhattan, Kansas State University, 108 p.

Hsü, K.J., 1969, Preliminary report and geologic guide to Franciscan mélanges of the Morro Bay-San Simeon area, California: California Division of Mines and Geology Special Publication 35, 46 p.

Jayko, A.S., Blake, M.C., Jr., and Harms, T., 1987, Attenuation of the Coast Range Ophiolite by extensional faulting, and nature of the Coast Range "Thrust," California: Tectonics, v. 6, p. 475-488.

Kusky, T.M., Bradley, D.C., and Haeussler, P., 1997, Progressive deformation of the Chugach accretionary complex, Alaska, during a Paleogene ridgetrench encounter: Journal of Structural Geology, v. 19, p. 139-157.

Lachenbruch, A.H., Sass, J.H., 1980, Heat flow and energetics of the San Andreas fault zone: Journal of Geophysical Research: Solid Earth, v. 85(B11), p. 6185-6222.

Lacroix B., Hughes, J., Lahfid, A., Spangenberg. J., Putlitz, B., Ward, C., Kempton, P.D., 2020, Structure and Origin of the Gold Mineralization in the Nacimiento Block: The Los Burros Deposit (Central California): Ore Geology review.

Lahfid, A., Beyssac, O., Deville, E., Negro, F., Chopin, C., and Goffé, B., 2010, Evolution of the Raman spectrum of carbonaceous material in low-grade metasediments of the Glarus Alps (Switzerland): Terra Nova, v. 22, no. 5, p. 354-360.

Lahfid, A., Delchini, S., and Lacroix, B., 2015, Contribution of the RSCM geothermometry to detect the thermal anomalies and peak temperatures induced by fluid circulation in metasediments, 13th SGA Biennial meeting.

Lori, L., 2016, Exhumation of the Nacimiento block: A thermochronological analysis [Master's thesis]: Rolla, Missouri University of Science and Technology, 138 p.

Niemi, N.A., and Clark, M.K., 2018, Long-term exhumation rates exceed paleoseismic slip rates in the central Santa Monica Mountains, Los Angeles County, California: Geology, v. 46, no. 1, p. 63-66, doi: 10.1130/G39388.1.

Page, B.M., 1970, Sur-Nacimiento fault zone of California: Continental margin tectonics: Geological Society of America Bulletin, v. 81, p. 668–690.

Pavlis, T.L., and Sisson, V.B., 1995, Structural history of the Chugach metamorphic complex in the Tana River region, eastern Alaska: A record of Eocene ridge subduction: Geological Society of America Bulletin, v. 107, p. 1333–1355.

Reiners, P.W., 2005, Zircon (U-Th)/He Thermochronometry: Reviews in Mineralogy and Geochemistry, v. 58, p. 151-179.

Reiners, P.W., Ehlers, T.A., and Zeitler, P.K., 2005, Past, Present, and Future of Thermochronology: Mineralogy and Geochemistry, v. 58, p. 1-18.

Reiners, P.W., Spell, T.L., Nicolescu, S., and Zanetti, K.A., 2004, Zircon (U-Th)/He thermochronometry: He diffusion and comparisons with $^{40}Ar/^{39}Ar$ dating: Geochimica et Cosmochimica Acta, v. 68, no. 8, p. 1857-1887.

Sadezky, A., Muckenhuber, H., Grothe, H., Niessner, R., and Pöschl, U., 2005, Raman microspectroscopy of soot and related carbonaceous materials: Spectral analysis and structural information: Carbon, v. 43, no. 8, p. 1731–1742.

Sisson, V.B., Hollister, L.S., and Onstott, T.C., 1989, Petrologic and age constraints on the origin of a low-pressure/high-temperature metamorphic complex, southern Alaska: Journal of Geophysical research, v. 94, p. 4392-4410.

Sorlien, C.C., Kamerling, M.J., and Mayerson, D., 1999, Block rotation and termination of the Hosgri strike-slip fault, California, from three-dimensional map restoration: Geology, v. 27, no. 11, p. 1039-1042.

Spotila, J. A., Farley, K. A., Yule, J. D., and Reiners, P. W., 2001, Near-field transpressive deformation along the San Andreas fault zone in southern California, based on exhumation constrained by (U-Th)/He dating: Journal of Geophysical Research, v. 106, no. B12, p. 30,909-30,922.

Steely, A.N., 2016, Fault-Controlled Patterns of Uplift in the Central California Coast Range and Laser-Ablation Depth-Profile Analysis of Zircon [Ph.D. thesis]: Santa Cruz, University of California, 205 p.

Storti, F., Billi, A., and Salvini, F., 2003, Particle size distributions in natural carbonate fault rocks: Insight for non-self-similar cataclasis: Earth and Planetary Science Letters, v. 206, p. 173-186.

Suppe, J., and Armstrong, R.L., 1972, Potassium argon dating of Franciscan metamorphic rocks: American Journal of Science, v. 272, p. 217-233.

Thorkelson, D.J., 1996, Subduction of diverging plates and the principles of slab window formation: Tectonophysics, v. 255, p. 47-63.

Ukar, E., 2012, Tectonic significance of low-temperature blueschist blocks in the Franciscan mélange at San Simeon, California: Tectonophysics, v. 568-569, p. 154-169, doi: 10.1016/j.tecto.2011.12.039.

Underwood, M.B., and Laughland, M.M., 2001, Paleothermal structure of the Point San Luis slab of central California: Effects of Late Cretaceous underplating, out-of-sequence thrusting, and late Cenozoic dextral offset: Tectonics, v. 20, no. 1, p. 97-111.

Underwood, M.B., Laughland, M.M., Shelton, K.L., and Sedlock, R.L., 1995, Thermal-maturity trends within Franciscan rocks near Big Sur, California: Implications for offset along the San Gregorio–San Simeon–Hosgri fault zone: Geology, v. 23, no. 9, p. 839-842.

Underwood, M.B., Shelton, K.L., McLaughlin, R.J., Laughland, M.M., Solomon, R.M., 1999, Middle Miocene paleotemperature anomalies within the Franciscan Complex of northern California: Thermo-tectonic responses near the Mendocino triple junction: Geological Society of America Bulletin, v. 111(10), p. 1448-1467.

Wills, C.J., Manson, M.W., Brown, K.D., Davenport, C.W., and Domrose, C.J., 2003, Landslides in the Highway 1 corridor between Point Lobos and San Luis Obispo Counties, California: California Geological Survey.

Zeitler, P.K., 2014, U-Th/He Dating: Encyclopedia of Scientific Dating Methods.

Appendix A - Analytical Data for (U-Th)/He Analysis

Table A.1 Analytical data for apatite (U-Th)/He thermochronology. All data processed at the University of Michigan Thermochronology Lab. LA-ICP-MS done at The University of Arizona, Arizona Radiogenic Helium Dating Laboratory.

Sample	Aliquot	Length (um)	Radius (um)	Shape*	U (ppm)	Th (ppm)	Sm (ppm)	He (2) (ncc)	Uncorrected Age (Ma)	Age Error (Ma)
NB19-015	a	148.9	50.8	nn	32.82	13.43	3.39	0.0608	4.3	0.06
	b	97.2	50.4	pp	5.58	16.64	2.35	0.0130	4.7	0.07
	c	130.8	51.0	np	7.63	12.41	3.57	0.0182	4.5	0.08
NB19-019	a	159.9	57.0	nn	1.90	4.57	0.36	0.0118	6.4	0.09
	b	132.5	61.6	np	4.76	12.59	2.63	0.0208	4.8	0.07
	c	117.0	43.3	pp	12.50	27.68	2.83	0.0174	3.7	0.05
NB19-021	b	178.0	46.4	nn	29.48	10.12	3.17	0.0571	4.6	0.06
	c	150.6	64.1	pp	9.35	30.67	0.92	0.0548	5.2	0.05
	e	147.5	55.7	pp	14.24	28.47	1.32	0.0428	4.3	0.06
	f	115.7	56.3	pp	23.80	74.05	1.94	0.0843	5.5	0.06
NB19-025	a	91.0	47.3	pp	16.04	9.41	0.87	0.0272	6.9	0.10
	b	132.5	51.0	np	35.36	5.44	0.39	0.0660	5.2	0.08
	c	140.0	52.6	np	14.30	20.02	1.02	0.0262	3.4	0.04
	d	104.7	42.0	np	78.71	41.06	1.40	0.1347	8.4	0.11
NB19-032	a	120.2	61.6	np	9.55	23.19	2.28	0.0220	2.9	0.04
	b	135.6	42.6	nn	90.33	173.75	2.26	0.1094	3.4	0.04
	c	86.6	41.7	pp	113.97	177.44	3.96	0.0585	2.5	0.03
	d	143.5	48.8	np	53.01	85.59	2.65	0.0678	2.7	0.03

*Shape abbreviations in relation to QTQt input: nn = sphere (2T), np = 1T Fragment, pp = 0T Fragment

Table A.2 Analytical data for zircon (U-Th)/He thermochronology. All data processed at the University of Michigan Thermochronology Lab. LA-ICP-MS done at The University of Arizona, Arizona Radiogenic Helium Dating Laboratory.

Sample	Aliquot	Length (um)	Radius (um)	Shape*	U (ppm)	Th (ppm)	Sm (ppm)	He (2) (ncc)	Uncorrected Age (Ma)	Age Error (Ma)
NB19 -004	a	150.6	40.2	nn	325.33	283.51	0.00	0.5187	5.6	0.07
	b	129.0	44.8	nn	441.15	349.12	0.00	1.2977	9.8	0.12
	c	102.9	43.3	nn	1158.47	686.11	0.00	2.5204	10.2	0.14
NB19 -015	a	230.2	51.7	nn	2219.99	1217.72	0.00	24.5553	16.4	0.22
	b	252.2	50.1	nn	328.70	299.01	0.00	5.1835	21.0	0.26
	c	217.8	56.3	nn	2087.89	1276.08	0.00	64.2698	39.9	0.51
NB19 -019	a	197.9	42.4	nn	1478.98	952.22	0.00	9.2204	15.6	0.19
	b	173.1	50.4	np	403.24	244.45	0.00	2.5035	12.7	0.16
	c	130.8	40.2	nn	830.84	707.43	0.00	3.7422	18.2	0.23
NB19 -021	a	220.4	52.3	nn	707.51	446.28	0.00	40.3463	83.9	1.04
	b	220.6	43.5	nn	960.30	572.79	0.00	28.5572	63.9	0.82
	c	191.7	52.3	nn	113.89	102.78	0.00	2.2330	31.5	0.39
NB19 -025	a	238.8	60.1	nn	434.57	142.75	0.00	26.2220	66.5	0.89
	b	225.3	53.9	nn	334.74	273.46	0.00	21.9108	85.6	1.04
	c	245.1	72.2	nn	282.54	184.87	0.00	21.7402	53.4	0.69
NB19 -032	a	148.9	48.6	nn	1561.89	1131.95	0.00	8.2448	13.2	0.17
	b	199.2	47.0	nn	1906.12	1176.92	0.00	6.2287	6.6	0.09
	c	159.9	41.1	nn	2030.08	1014.55	0.00	6.4556	10.8	0.14

*Shape abbreviations in relation to QTQt input: nn = sphere (2T), np = 1T Fragment, pp = 0T Fragment